The class IA phosphatidylinositol 3-kinase p110-β subunit is a positive regulator of autophagy

Zhixun Dou,[1] Mohar Chattopadhyay,[2] Ji-An Pan,[1] Jennifer L. Guerriero,[1] Ya-Ping Jiang,[3] Lisa M. Ballou,[3] Zhenyu Yue,[4] Richard Z. Lin,[2,3,5] and Wei-Xing Zong[1]

[1]Departments of Molecular Genetics & Microbiology, [2]Physiology and Biophysics, and [3]Medicine, Stony Brook University, Stony Brook, NY 11794
[4]Department of Neurology and Neuroscience, Mt. Sinai School of Medicine, New York, NY 10029
[5]Department of Veterans Affairs Medical Center, Northport, NY 11768

Autophagy is an evolutionarily conserved cell renewal process that depends on phosphatidylinositol 3-phosphate (PtdIns(3)P). In metazoans, autophagy is inhibited by PtdIns(3,4,5)P_3, the product of class IA PI3Ks, which mediates the activation of the Akt–TOR kinase cascade. However, the precise function of class IA PI3Ks in autophagy remains undetermined. Class IA PI3Ks are heterodimeric proteins consisting of an 85-kD regulatory subunit and a 110-kD catalytic subunit. Here we show that the class IA p110-β catalytic subunit is a positive regulator of autophagy. Genetic deletion of p110-β results in impaired autophagy in mouse embryonic fibroblasts, liver, and heart. p110-β does not promote autophagy by affecting the Akt–TOR pathway. Rather, it associates with the autophagy-promoting Vps34–Vps15–Beclin 1–Atg14L complex and facilitates the generation of cellular PtdIns(3)P. Our results unveil a previously unknown function for p110-β as a positive regulator of autophagy in multicellular organisms.

Introduction

The phosphatidylinositol 3-kinases (PI3Ks) are lipid kinases that phosphorylate the 3′-hydroxyl group of phosphatidylinositol (PtdIns) and phosphoinositides. The generated phospholipids are critical signaling molecules. Based on substrate specificity and sequence homology, PI3Ks are grouped into three classes: class I, class II, and class III (Domin and Waterfield, 1997). Class I PI3Ks are divided into two groups, class IA and class IB. Class IA PI3Ks respond to both receptor tyrosine kinases (RTKs) and G protein–coupled receptors (GPCRs). They are heterodimeric proteins consisting of an 85-kD regulatory subunit and one of the three 110-kD catalytic subunits (p110-α, p110-β, and p110-δ; Fruman et al., 1998; Cantley, 2002; Engelman et al., 2006; Hawkins et al., 2006). In vivo, class I PI3Ks are believed to preferentially phosphorylate PtdIns(4,5)P_2 to generate PtdIns(3,4,5)P_3, a pivotal signaling molecule that activates multiple downstream signaling cascades, including the Akt–TOR pathway (Fruman et al., 1998; Cantley, 2002; Sarbassov et al., 2005; Engelman et al., 2006; Hawkins et al., 2006).

Class III PI3K is composed of a sole member, Vps34, that converts PtdIns to PtdIns(3)P. Vps34 is the only PI3K reported to be evolutionarily conserved from yeast to mammals (Vanhaesebroeck et al., 2001; Backer, 2008). Vps34 exerts its lipid kinase activity by forming a protein complex with a putative Ser–Thr protein kinase Vps15. The interaction with Vps15 targets Vps34 to intracellular membranes and mediates the localized production of PtdIns(3)P that is essential for endocytic trafficking, and phagosome formation and maturation (Vanhaesebroeck et al., 2001; Backer, 2008).

A major cellular event regulated by PI3Ks is autophagy (Petiot et al., 2000). Autophagy involves the sequestration of cellular constituents including macromolecules and organelles into double-membrane structures termed autophagosomes that later fuse with acidified late endosomes and lysosomes, leading to degradation of the enclosed constituents by lysosomal hydrolases (Levine and Yuan, 2005; Lum et al., 2005; Klionsky et al., 2008;

Correspondence to Wei-Xing Zong: wzong@notes.cc.sunysb.edu

Abbreviations used in this paper: GPCR, G protein–coupled receptor; LC, light chain; MEF, mouse embryonic fibroblast; PI3K, phosphatidylinositol 3-kinase; PtdIns(3)P, phosphatidylinositol 3-phosphate; RTK, receptor tyrosine kinase; TAC, transverse aortic constriction.

The Rockefeller University Press $30.00
J. Cell Biol. Vol. 191 No. 4 827–843
www.jcb.org/cgi/doi/10.1083/jcb.201006056

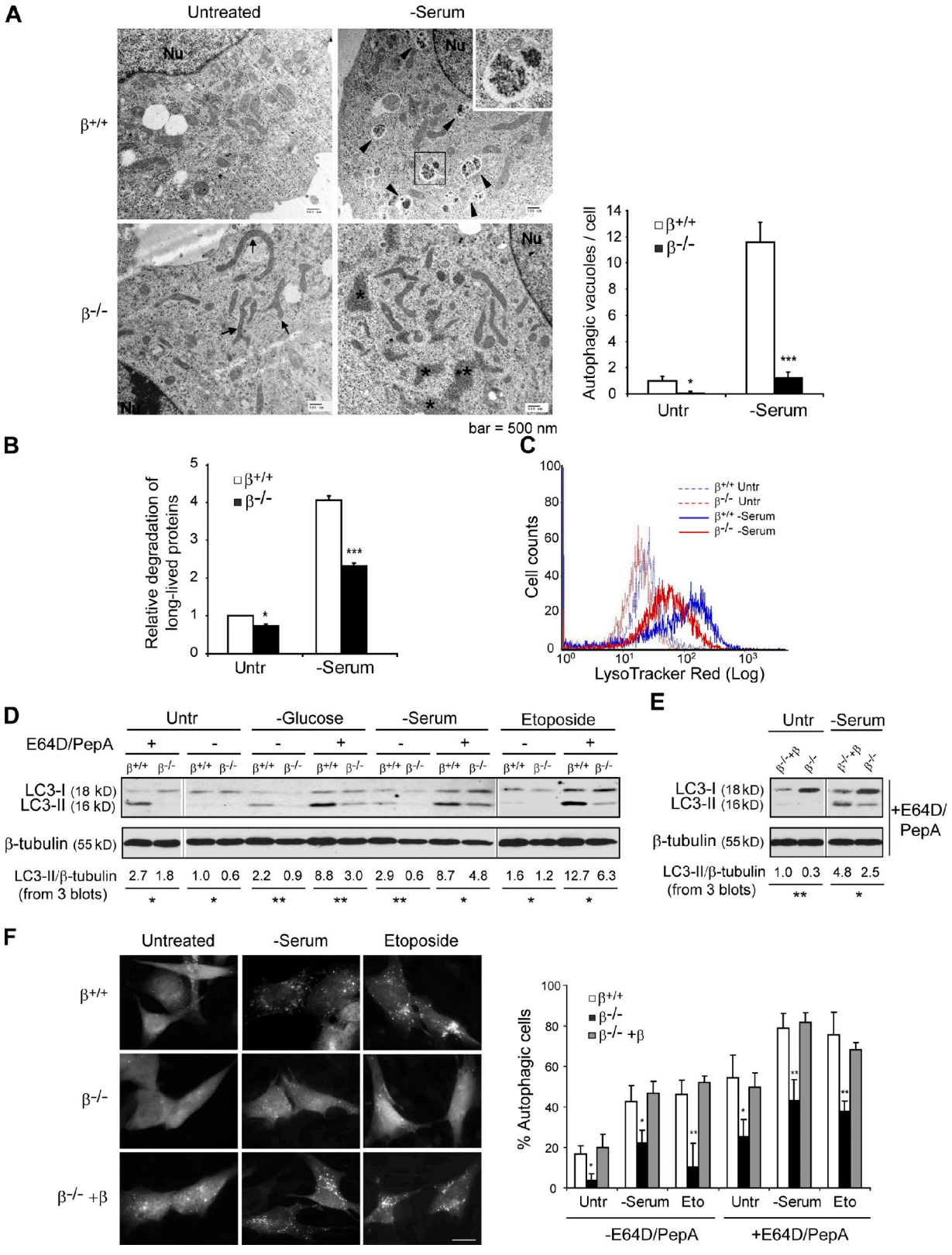

Figure 1. **Autophagy is impaired in $\beta^{-/-}$ MEFs.** (A) $\beta^{+/+}$ and $\beta^{-/-}$ MEFs were cultured in complete (untreated) or serum-free medium for 6 h, then observed under an electron microscope. Note the appearance of autophagosomes in serum-deprived $\beta^{+/+}$ MEFs, indicated by arrowheads. A higher magnification view of an autophagosome is shown in the inset. In $\beta^{-/-}$ MEFs, deformed mitochondria are indicated by arrows. In serum-deprived $\beta^{-/-}$ MEFs, aggregated ribosomes are indicated by asterisks. Nu, nucleus. (Right) Quantification of autophagic vacuoles per cell. Error bars = SEM; $n = 10$; *, $P < 0.05$; ***, $P < 0.0001$. (B) MEFs were labeled with ^{14}C-valine for 24 h and cultured in complete or serum-free medium for 6 h. Degradation of long-lived proteins was measured and normalized. Data presented are averages of three independent experiments ± SEM; *, $P < 0.05$; ***, $P < 0.0001$. (C) MEFs were cultured in complete or serum-free medium for 6 h. Cells were stained with LysoTracker red and subjected to flow cytometry analysis. Data shown are representative

Levine and Kroemer, 2008; Mizushima et al., 2008). During autophagy, the Vps34–Vps15 complex is diverted to autophagosome-specific intracellular membrane compartments by associating with a number of proteins including Beclin 1 and Atg14L (also known as Barkor; Kihara et al., 2001; Sun et al., 2008; Matsunaga et al., 2009; Simonsen and Tooze, 2009; Zhong et al., 2009). This leads to localized production of PtdIn(3)P that recruits proteins containing FYVE domains and PX domains to the preautophagosomal membrane structure and triggers autophagy (Lindmo and Stenmark, 2006; Axe et al., 2008; Juhász et al., 2008; Simonsen and Tooze, 2009). In contrast to Vps34, the class IA PI3Ks are implicated in the inhibition of autophagy (Petiot et al., 2000), primarily by activating the Akt–TOR pathway that disrupts the autophagy-essential Atg1–Atg17–Atg13 complex (Levine and Kroemer, 2008; Chang et al., 2009). Hence, the current understanding is that class IA PI3Ks play an inhibitory role in autophagy by producing PtdIns(3,4,5)P_3 that activates the Akt–TOR kinase pathway, whereas class III PI3K plays a stimulatory role by producing PtdIns(3)P that is essential for autophagosome formation. However, a direct function of the class IA PI3Ks on autophagy remains undetermined. Here, we use conditional gene knockout mice deficient in the class IA PI3K p110-α or p110-β catalytic subunit (Lu et al., 2009) to study their involvement in the regulation of autophagy.

Results

p110-$\beta^{-/-}$ mouse embryonic fibroblasts have impaired autophagy

Mouse embryonic fibroblasts (MEFs) were isolated from *p110*-$\alpha^{flox/flox}$ and *p110*-$\beta^{flox/flox}$ mice (Lu et al., 2009) and immortalized using SV40 large T antigen. Expression of the Cre recombinase in *p110*-$\alpha^{flox/flox}$ or *p110*-$\beta^{flox/flox}$ MEFs resulted in virtually complete loss of p110-α or p110-β protein, respectively (Fig. S1 A). We hereafter refer to the flox/flox MEFs without Cre recombination as $\alpha^{+/+}$ or $\beta^{+/+}$ MEFs, and the knockout cells as $\alpha^{-/-}$ or $\beta^{-/-}$ MEFs. The steady-state level of p85 was not affected in $\alpha^{-/-}$ or $\beta^{-/-}$ MEFs (Fig. S1 A). Consistent with previous reports (Zhao et al., 2006; Guillermet-Guibert et al., 2008; Jia et al., 2008), $\alpha^{-/-}$ MEFs showed a significant decrease in Akt phosphorylation in response to RTK signaling such as that triggered by EGF, PDGF, and insulin (Fig. S1 B), whereas $\beta^{-/-}$ MEFs were defective in GPCR signaling triggered by lysophosphatidic acid (LPA; Fig. S1, C and D).

When observed by electron microscopy (EM), $\beta^{+/+}$ MEFs upon serum deprivation displayed an increase in double-layered membrane structures enclosing electron-dense material, characteristic of autophagosomes (Fig. 1 A). In sharp contrast, $\beta^{-/-}$ MEFs failed to show autophagosome formation upon serum deprivation. Rather, deformed mitochondria and accumulation of ribosome aggregates were observed in $\beta^{-/-}$ MEFs (Fig. 1 A), consistent with previous observations made in autophagy-deficient cells (Komatsu et al., 2005; Kraft et al., 2008; Kundu et al., 2008). To confirm a defect in autophagy, we examined the autophagy-mediated degradation of long-lived proteins, as well as the lysosomal activity that is associated with autophagy using the pH-dependent lysosomal dye LysoTracker red. $\beta^{+/+}$ MEFs showed a higher basal level of long-lived protein degradation and lysosomal activity than $\beta^{-/-}$ MEFs (Fig. 1, B and C). Serum deprivation further enhanced the long-lived protein degradation and lysosomal activity in $\beta^{+/+}$ MEFs, but the enhancement was markedly impaired in $\beta^{-/-}$ MEFs (Fig. 1, B and C).

To further determine the effect of *p110-β* gene deletion on autophagy, we exposed the MEFs, in the absence or presence of lysosomal peptidase inhibitors E64D and pepstatin A (Klionsky et al., 2008; Mizushima et al., 2010), to a number of known autophagy-inducing conditions including glucose deprivation, serum deprivation, and the DNA-damaging agent etoposide. The conversion of microtubule-associated protein 1 light chain 3 (LC3) from its cytosolic form (LC3-I) to a membrane-bound form (LC3-II) was examined as a molecular marker for autophagosomal formation. All autophagy-inducing conditions resulted in accumulation of LC3-II in $\beta^{+/+}$ cells, whereas the accumulation of LC3-II was markedly lower in $\beta^{-/-}$ MEFs (Fig. 1 D). Reconstitution of $\beta^{-/-}$ MEFs with p110-β restored LC3 conversion (Fig. 1 E). The inconsistency of the intensity of LC3-I in the immunoblots throughout the study was noted. This is possibly due to the various batches of LC3 antibodies from different resources. Nevertheless, we normalized the intensity of LC3-II against that of β-tubulin to determine autophagy induction. In addition to the LC3 immunoblot analysis, the ability of GFP-tagged LC3 to form autophagic puncta has been used to monitor autophagy (Kabeya et al., 2000). $\beta^{+/+}$ and p110-β–reconstituted $\beta^{-/-}$ MEFs expressing GFP-LC3 showed a change from a diffuse pattern to a punctate pattern upon autophagic stimuli, whereas both the size and number of GFP-LC3 puncta were markedly reduced in $\beta^{-/-}$ MEFs (Fig. 1 F). In agreement with the positive role of p110-β in autophagy, knockdown of p110-β by shRNA in HEK293 cells resulted in accumulation of p62/SQSTM1, as well as impaired LC3-II formation (Fig. S2, A and B).

In contrast to $\beta^{-/-}$ MEFs, $\alpha^{-/-}$ MEFs showed similar or slightly enhanced autophagy compared with $\alpha^{+/+}$ MEFs, as indicated by EM (Fig. S3 A), LysoTracker red staining (Fig. S3 B), LC3 conversion (Fig. S3 C), and GFP-LC3 puncta formation (Fig. S3 D). Taken together, these results demonstrated that p110-β, but not p110-α, is required for autophagy.

of three independent experiments. (D) MEFs were cultured in glucose-free medium for 12 h, serum-free medium for 6 h, or treated with 25 µM etoposide for 6 h in the presence or absence of lysosomal inhibitors E64D and PepA. Cell lysates were probed for LC3 and β-tubulin. Quantification of LC3-II/β-tubulin from three independent immunoblots is shown. Data presented are the mean values normalized to $\beta^{+/+}$ untreated condition. *, $P < 0.05$; **, $P < 0.005$. (E) $\beta^{-/-}$ and p110-β–reconstituted $\beta^{-/-}$ MEFs were left untreated or serum starved for 6 h in the presence of E64D and PepA. Cell lysates were subjected to LC3 and β-tubulin immunoblotting. Quantification of LC3-II/β-tubulin from three independent experiments is shown. *, $P < 0.05$; **, $P < 0.005$. (F) MEFs with indicated genotypes expressing GFP-LC3 were treated as indicated. Cells were observed under a deconvolution fluorescence microscope. Representative images are shown. Quantification of autophagic cells was determined as described in Materials and methods. Data shown are averages of at least five blind countings ± SD. *, $P < 0.05$; **, $P < 0.005$. Bar, 20 µm.

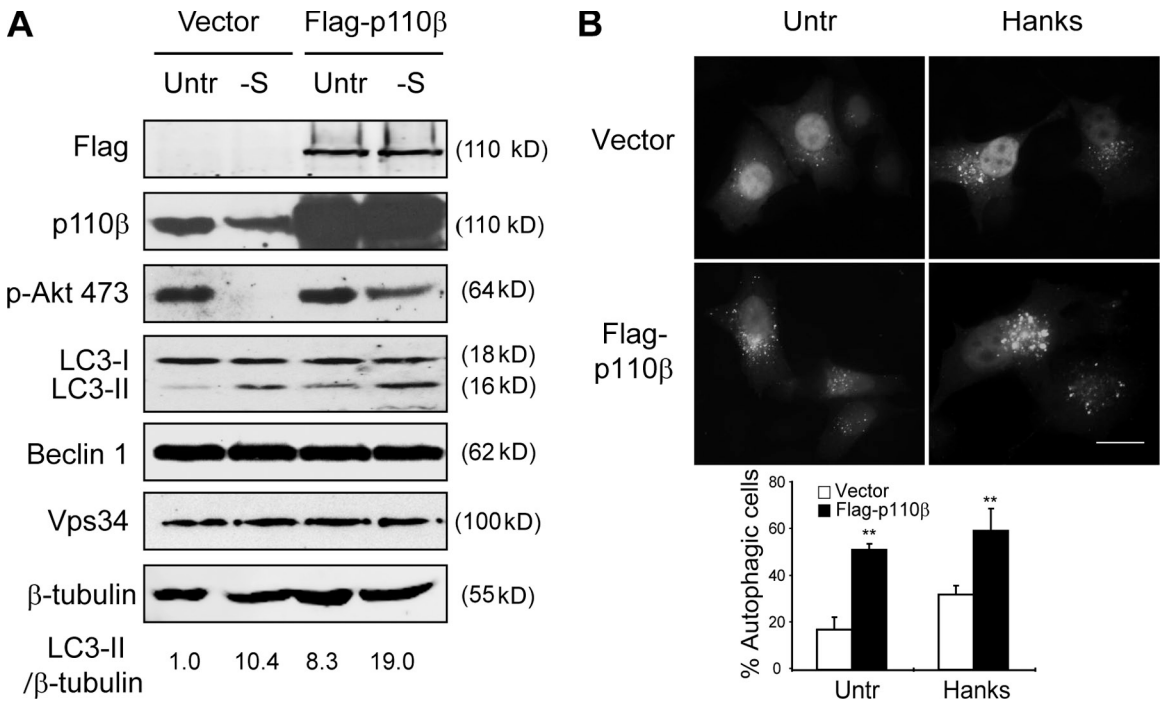

Figure 2. **Overexpression of p110-β stimulates autophagy.** (A) HEK293 cells were transfected with vector or Flag–p110-β expression construct. 48 h after transfection, cells were left untreated or serum starved for 12 h. Cell lysates were immunoblotted with indicated antibodies. Quantification of the relative LC3-II/β-tubulin ratio is shown. (B) HeLa cells were transfected with GFP-LC3 construct, together with empty vector or Flag–p110-β expression construct. 48 h after transfection, cells were cultured in complete medium or in Hank's buffer for 4.5 h. Cells were fixed and observed under a fluorescence microscope. Representative images were taken, and quantification of autophagic cells is shown. Data presented are average of four blind countings ± SD. **, $P < 0.005$. Bar, 20 µm.

Ectopic expression of p110-β stimulates autophagy

To examine the converse of *p110-β* gene deletion, Flag-tagged p110-β was ectopically expressed in HEK293 cells. With serum deprivation, the p110-β–overexpressing cells maintained higher Akt phosphorylation than control cells (Fig. 2 A). Despite the elevated Akt phosphorylation, the amount of LC3-II was significantly higher in cells expressing Flag–p110-β, whereas the steady-state levels of the key autophagy regulators Beclin 1 and Vps34 remained unchanged (Fig. 2 A). In another HEK293 line where we stably expressed GFP-LC3, overexpression of p110-β, but not p110-α, enhanced the generation of GFP–LC3-II (Fig. S2 C). In addition, an increased amount of the cleaved free-GFP was observed in Flag-p110-β–expressing cells, suggesting an enhanced autophagy flux (Fig. S2 C). Similarly, expression of Flag–p110-β markedly increased the number and size of GFP-LC3 puncta both at the basal state and upon nutrient starvation in HeLa cells (Fig. 2 B). These results support a stimulatory role of p110-β in autophagy, and suggest that the autophagy-promoting role of p110-β is dominant over the inhibitory effect imposed by elevated Akt activity.

p110-β does not act through the Akt–TOR pathway to promote autophagy

The canonical PI3K–Akt–TOR pathway plays an inhibitory role in autophagy (Lindmo and Stenmark, 2006; Levine and Kroemer, 2008). However, our observation above suggested that p110-β positively regulates both Akt and autophagy (Fig. 2 A). One explanation for this apparent paradox is that p110-β has two distinct functions: one is to promote Akt activation, and the other to promote autophagy. We went on to examine whether inhibition of Akt and TOR can induce autophagy in the absence of p110-β. $\beta^{+/+}$ and $\beta^{-/-}$ MEFs were treated with pharmacological inhibitors of Akt (Akti) or TOR (rapamycin). In $\beta^{+/+}$ MEFs growing in complete medium, both inhibitors stimulated autophagy as indicated by LC3 conversion (Fig. 3 A) and GFP-LC3 puncta formation (Fig. 3, B and C), and the induction of autophagy was further enhanced when cells were deprived of glucose or serum (Fig. 3 A). In sharp contrast, autophagy induced by Akt and TOR inhibitors was dramatically reduced in $\beta^{-/-}$ MEFs under all of these conditions (Fig. 3, A–C). The failure of p110-β kinase–specific inhibitor TGX-221 to inhibit autophagy (Fig. 3 A) suggests that p110-β kinase activity may not be required for regulating autophagy, a point we will discuss later. Together with our finding that overexpression of p110-β could stimulate Akt phosphorylation and autophagy simultaneously (Fig. 2 A), these data indicate that p110-β–mediated autophagy is independent of Akt–TOR signaling.

p110-β modulates the level of cellular PtdIns(3)P and Vps34 catalytic activity

We next determined the molecular mechanisms through which p110-β regulates autophagy. The steady-state levels of the key autophagy regulators Vps34, Beclin 1, Atg14L, and Rubicon appeared unaltered in $\beta^{-/-}$ MEFs (Fig. S4 A), and the expression levels of Beclin 1, Vps34, and Rubicon remained unaltered

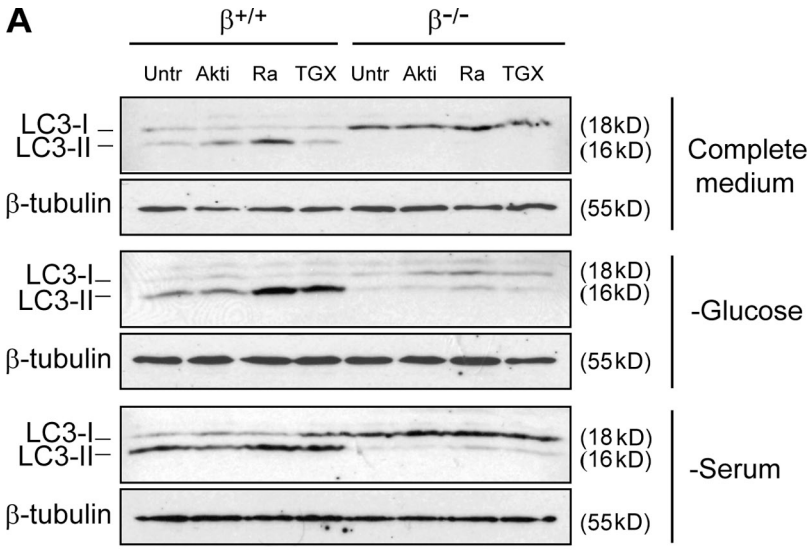

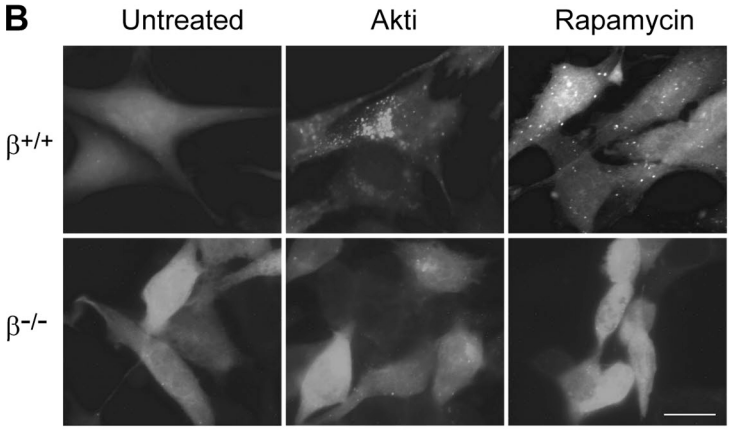

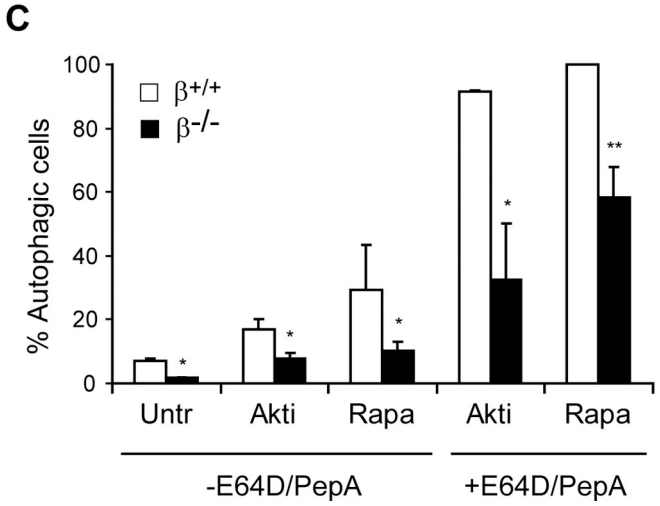

Figure 3. **p110-β promotes autophagy independently of the Akt–TOR pathway.** (A) $\beta^{+/+}$ and $\beta^{-/-}$ MEFs were left untreated or treated with 5 μM Akt inhibitor (Akti), 20 nM rapamycin (Ra), or 500 nM TGX-221 (TGX, pretreated overnight) in complete medium or in combination with glucose deprivation (12 h), or serum deprivation (6 h), all in the presence of lysosomal inhibitors E64D and PepA. Cell lysates were immunoblotted for LC3 and β-tubulin. (B) $\beta^{+/+}$ and $\beta^{-/-}$ MEFs stably expressing GFP-LC3 were treated with 5 μM Akti or 20 nM rapamycin for 12 h. Cells were observed under a deconvolution fluorescence microscope. Representative images are shown. Bar, 20 μm. (C) Quantification of autophagic cells in MEFs stably expressing GFP-LC3 in response to indicated treatments. Data shown are averages of at least three blind countings ± SD. *, $P < 0.05$; **, $P < 0.005$.

in $\beta^{-/-}$ livers (Fig. S4 B). The decreased lysosomal acidification in $\beta^{-/-}$ MEFs (Fig. 1 C), however, indicated a possible deficiency in endosomal and lysosomal maturation in these cells. In fact, expression of a GFP-conjugated FYVE domain that specifically binds to PtdIns(3)P on endosomes and indicates endo-lysosomal activities revealed decreased GFP puncta in $\beta^{-/-}$ MEFs compared with $\beta^{+/+}$ MEFs (Fig. 4 A). This finding suggests that $\beta^{-/-}$ MEFs have decreased level of PtdIns(3)P, a lipid that is required for autophagy. To test this, we used a protein–lipid overlay assay to measure the intracellular level of PtdIns(3)P. The specificity of the assay was confirmed using a number of different PtdIns species as negative controls, and by treating

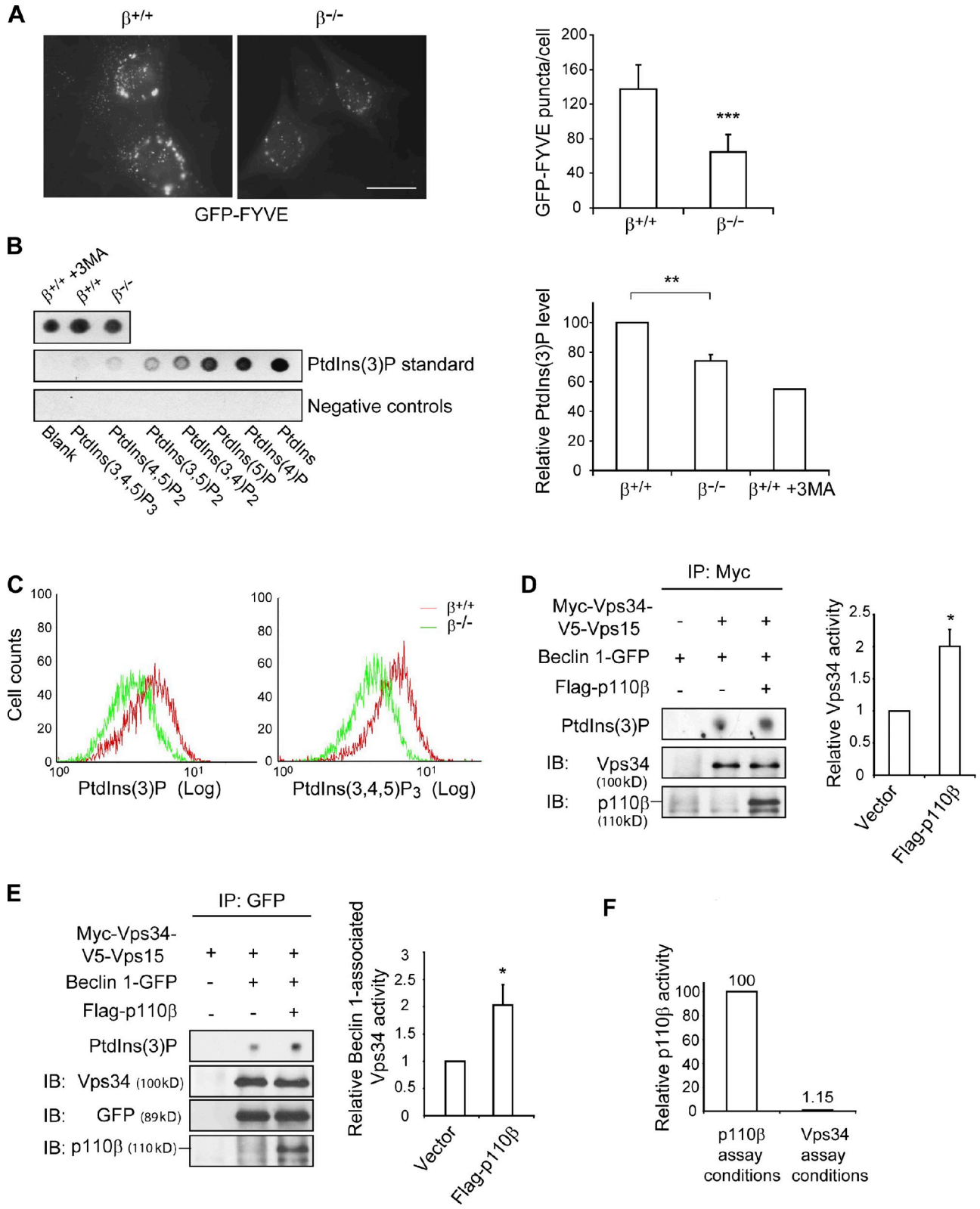

Figure 4. **p110-β positively regulates PtdIns(3)P level and Vps34 catalytic activity.** (A) $\beta^{+/+}$ and $\beta^{-/-}$ MEFs stably expressing GFP-FYVE were observed under a deconvolution fluorescence microscope. Representative images (left) and quantification of GFP-FYVE puncta per cell (right) are shown. Bar, 20 µm. ***, $P < 0.0001$; $n > 20$; error bars = SEM. (B) Total cellular lipids were extracted from $\beta^{+/+}$, $\beta^{-/-}$, and $\beta^{+/+}$ MEFs treated with 1 mM 3-MA for 12 h. The lipid extracts were subjected to protein–lipid overlay analysis for PtdIns(3)P content. PtdIns(3)P standard and other PtdIns species were used as controls. Data shown are representative of three independent experiments. Quantification of total cellular PtdIns(3)P normalized against total protein is shown on the right ($n = 3$ for $\beta^{+/+}$ and $\beta^{-/-}$; $n = 2$ for $\beta^{+/+}$ +3-MA; **, $P < 0.005$; error bars = SEM). (C) $\beta^{+/+}$ and $\beta^{-/-}$ MEFs were stained with antibodies against PtdIns(3)P or PtdIns(3,4,5)P_3, and subjected to flow cytometry analysis. (D and E) HEK293T cells were transfected with indicated plasmids. 48 h after transfection, cell lysates were subjected to immunoprecipitation using Myc antibody-conjugated agarose (D) or GFP antibody and protein A–conjugated

cells with 3-methyladenine (3-MA), a pharmacological inhibitor of Vps34 that resulted in a decreased level of intracellular PtdIns(3)P (Fig. 4 B). A decrease of ∼30% in the steady-state level of PtdIns(3)P was detected in $\beta^{-/-}$ MEFs as compared with $\beta^{+/+}$ cells (Fig. 4 B). Reconstitution of p110-β in $\beta^{-/-}$ MEFs restored PtdIns(3)P levels (Fig. 7 E). The decreased amount of PtdIns(3)P in $\beta^{-/-}$ MEFs was also detected by flow cytometry using a PtdIns(3)P-specific antibody, similar to the decreased level of PtdIns(3,4,5)P_3 in the $\beta^{-/-}$ MEFs (Fig. 4 C).

Vps34 is the predominant kinase that produces intracellular PtdIns(3)P and promotes autophagy, as part of a complex with Vps15 and Beclin 1 (Simonsen and Tooze, 2009). We thus examined if p110-β affects PtdIns(3)P levels by modulating Vps34 activity. The bicistronic Myc–Vps34–V5–Vps15 expression construct (Yan et al., 2009) and the Beclin 1–GFP construct were cotransfected into HEK293T cells with or without Flag–p110-β. Vps34 kinase activity was then assayed in anti-Myc or anti-GFP immunoprecipitates using PtdIns as a substrate. In both assays, Vps34 kinase activity was enhanced in the presence of p110-β (Fig. 4, D and E). The increased conversion of PtdIns to PtdIns(3)P in the assay was not due to phosphorylation of PtdIns by p110-β because p110-β exhibits little kinase activity in the assay conditions used to measure Vps34 activity (Fig. 4 F). Taken together, these results indicate that p110-β promotes Vps34 kinase activity and PtdIns(3)P production, a process prerequisite for autophagosome formation.

p110-β is required for the early stage of autophagosome formation

PtdIns(3)P is known to regulate both endocytic and autophagic pathways (Burman and Ktistakis, 2010). As we observed that the PtdIns(3)P level and autophagy are lower in $\beta^{-/-}$ cells, we went on to determine whether the autophagic pool of PtdIns(3)P is affected by p110-β. DFCP1 (double FYVE domain–containing protein 1) has recently been shown to relocalize from the ER/Golgi to omegasome, the precursor membrane structure of autophagosome, in a PtdIns(3)P-dependent manner upon autophagy induction (Axe et al., 2008). To test if the formation of the omegasome structure is affected in the $\beta^{-/-}$ MEFs, we expressed GFP-DFCP1 in $\beta^{+/+}$ and $\beta^{-/-}$ MEFs. Under fed state, $\beta^{+/+}$ MEFs displayed a diffuse pattern of GFP-DFCP1, which turned into a punctuate pattern upon serum starvation or Hank's buffer treatment (Fig. 5 A), consistent with previous reports (Axe et al., 2008; Polson et al., 2010). In contrast, under fed condition, $\beta^{-/-}$ MEFs showed an accumulation of GFP-DFCP1 puncta, which appeared to form aggregates that differed from the starvation-induced puncta in $\beta^{+/+}$ MEFs (Fig. 5 A). The accumulation of the abnormal GFP-DFCP1 puncta in $\beta^{-/-}$ cells is reminiscent of that observed in cells deficient in WIPI2, which is localized to omegasomes and promotes LC3 lipidation (Polson et al., 2010). Importantly, upon starvation, the amount of GFP-DFCP1 puncta in $\beta^{-/-}$ MEFs was significantly lower than that in $\beta^{+/+}$ MEFs (Fig. 5 A), indicating a deficient autophagy pool of PtdIns(3)P in $\beta^{-/-}$ MEFs. Consistent with this, another PtdIns(3)P-dependent event during early autophagosome formation, Atg5–Atg12 conjugation (Ravikumar et al., 2008), was also compromised in $\beta^{-/-}$ MEFs (Fig. 5 B).

To further confirm the early stage of autophagy influx is deficient in $\beta^{-/-}$ MEFs, we expressed the mCherry–GFP-LC3 construct in our MEFs. Owing to the more stable nature of mCherry than GFP in the acidified compartment, the relative amount of the yellow puncta (represent autophagosomes as a result of the merged green and red signals) and the red puncta (represent autolysosomes) can be used to indicate whether the early or late steps of the autophagic flux are affected (Mizushima et al., 2010). $\beta^{-/-}$ MEFs displayed significantly less yellow and red puncta than $\beta^{+/+}$ MEFs, in both basal state and under serum deprivation (Fig. S4 C). These data indicate that the lower PtdIns(3)P level in $\beta^{-/-}$ MEFs has a major impact on the early stage of autophagosome formation. In line with these observations, the $\beta^{-/-}$ livers displayed significantly less Beclin 1–GFP puncta upon fasting (Fig. S5), supporting a defect in the early stage of autophagosome formation that is mediated by Beclin 1–Atg14L interaction (Sun et al., 2008; Matsunaga et al., 2009; Zhong et al., 2009).

p110-β is a component of the autophagy-promoting Vps34–Vps15–Beclin 1–Atg14L complex

In mammalian cells, the autophagy-essential PtdIns(3)P is known to be produced by the Vps34–Vps15–Beclin 1 complex. It has been recently reported that Rab5 can also participate in the autophagosome formation through its interaction with the Vps34–Beclin 1 complex (Ravikumar et al., 2008). p110-β, but not p110-α, has been reported to directly associate with Rab5 (Christoforidis et al., 1999). These studies suggested to us that p110-β may participate in autophagy induction as part of the Rab5–Vps34–Beclin1 complex. Indeed, in the Vps34 assays, p110-β was observed to coprecipitate with Vps34 (Fig. 4 D) and Beclin 1 (Fig. 4 E). We confirmed that Rab5 immunoprecipitation was able to bring down overexpressed Vps15 and Vps34, as well as Flag–p110-β (Fig. 6 A). Furthermore, Rab5 pulled down endogenous p110-β, but not p110-α (Fig. 6 B). We then went on to test whether p110-β associates with the Vps34–Vps15–Beclin 1 complex. We found that Vps34 immunoprecipitation pulled down Vps15 and p110-β (Fig. 6 C), and likewise, p110-β immunoprecipitation pulled down Vps15 and Vps34 (Fig. 6 D). Vps15 immunoprecipitation pulled down Vps34 and p110-β, but not p110-α (Fig. 6 E). The presence of p110-β in the Vps34–Vps15 complex appeared unchanged or slightly

agarose (E). 75% of the precipitates were assayed for Vps34 catalytic activity, and 25% of the precipitates were immunoblotted with indicated antibodies. Vps34 activity is calculated as the amount of PtdIns(3)P generated normalized against the amount of Vps34 present in the precipitates. IP reaction using IgG isotype control showed no activity over the background scintillation readings. Representative autoradiographs of the in vitro Vps34 assay results and the corresponding immunoblots are shown on the left. Quantification of Vps34 activity and Beclin 1–associated Vps34 activity are shown on the right. Data shown are average of three independent experiments ± SEM. *, $P < 0.05$. (F) Purified p110-β/p85-α was assayed under p110-β or Vps34 assay conditions. Results shown are the average of duplicate experiments.

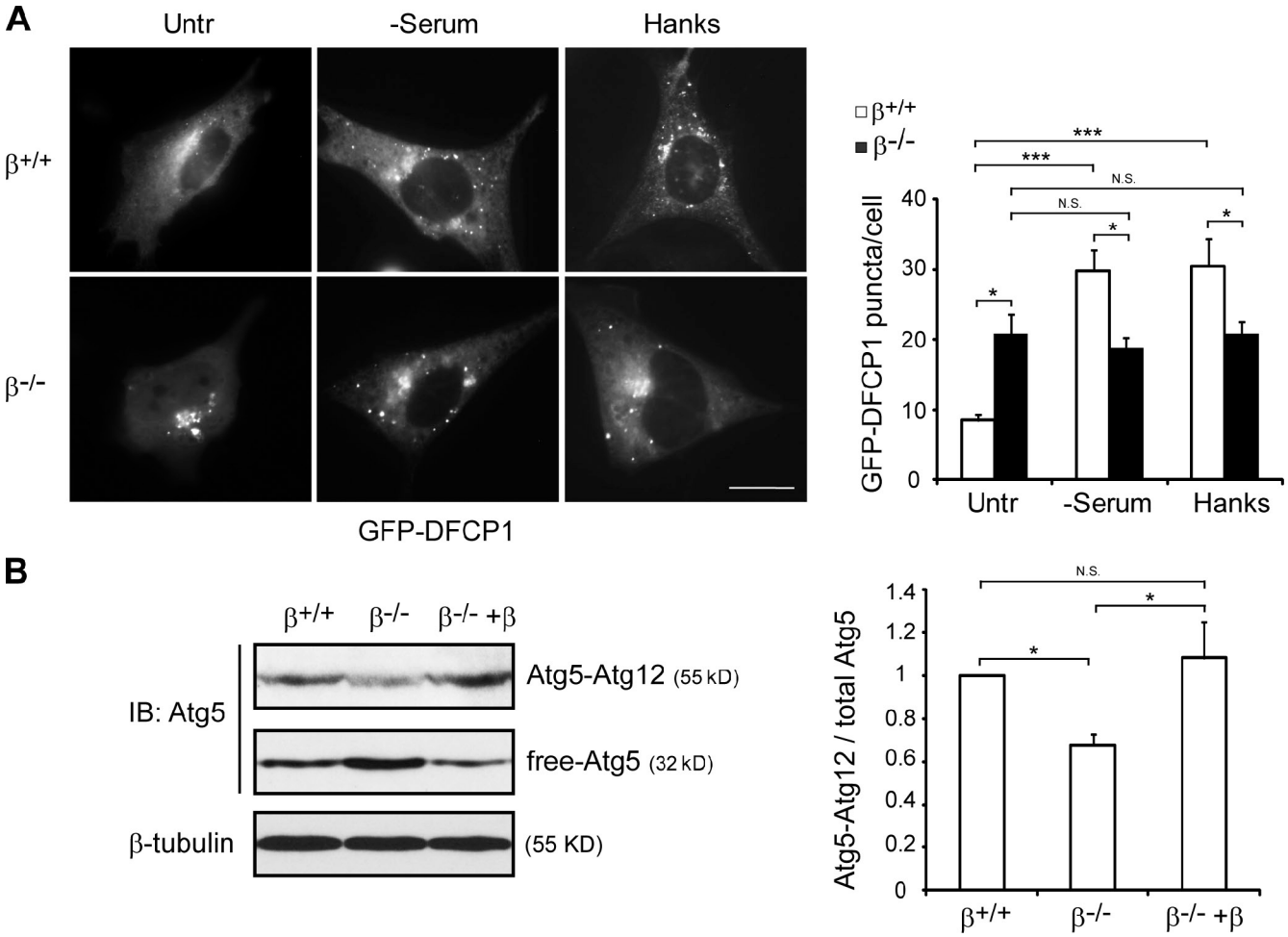

Figure 5. **Early stage of autophagosome formation is suppressed in $\beta^{-/-}$ MEFs.** (A) $\beta^{+/+}$ and $\beta^{-/-}$ MEFs were transfected with GFP-DFCP1 expression construct. 24 h after transfection, cells were cultured in complete medium, serum-free medium (6 h), or Hank's buffer (2 h). Cells were fixed, observed, and imaged under a deconvolution fluorescence microscope. Only cells with moderate levels of GFP signal were quantified and imaged. Representative images are shown. Bar, 20 µm. Quantification of GFP puncta per cell is shown on the right. Error bars = SEM; n = 10; *, $P < 0.05$; ***, $P < 0.001$; N.S., nonsignificant. (B) $\beta^{+/+}$, $\beta^{-/-}$, and p110-β–reconstituted $\beta^{-/-}$ MEFs lysates were probed for Atg5 and β-tubulin antibodies. The quantification of relative Atg5–Atg12 conjugation is shown on right. Data shown are the mean values from three independent experiments (*, $P < 0.05$; N.S., nonsignificant; error bars = SEM).

enhanced upon serum deprivation (Fig. 6, C and D). We also detected interaction between endogenous p110-β and Beclin 1 by immunoprecipitation (Fig. 6, F and G). Further studies with endogenous proteins were not done due to the limitation of available antibodies for Vps34 and Vps15 immunoprecipitations.

The Vps34–Vps15–Beclin 1 complex has been shown to interact with different partners and act at distinct stages of the autophagy pathway. The complex with Atg14L is known to promote autophagosome initiation, whereas the complex with UVRAG and Rubicon mainly regulates autophagosome maturation (Liang et al., 2008; Sun et al., 2008; Matsunaga et al., 2009; Simonsen and Tooze, 2009; Zhong et al., 2009). We thus asked whether p110-β interacts with the Atg14L, or UVRAG and Rubicon-containing complexes. We used the human p110-β–reconstituted $\beta^{-/-}$ MEFs to perform immunoprecipitation because our Atg14L and Rubicon antibodies preferentially recognize mouse antigens, whereas our p110-β antibody preferentially recognizes human p110-β. We found that p110-β immunoprecipitation pulled down Atg14L, but not UVRAG or Rubicon (Fig. 6 H). Likewise, Atg14L, but not Rubicon immunoprecipitation was able to bring down p110-β (Fig. 6 I). Immunofluorescence analysis confirmed that p110-β colocalized at least partially with Atg14L, both at fed and starved conditions (Fig. 6 J). Taken together, these data demonstrate that p110-β associates and colocalizes with the autophagy-promoting Vps34–Vps15–Beclin 1–Atg14L complex that generates PtdIns(3)P and is required for autophagosome initiation.

p110-β promotes autophagy and PtdIns(3)P production independently of its kinase activity

It has been reported that p110-β associates with a protein complex containing PtdIns 4- and 5-phosphatases that dephosphorylate PtdIns(3,4,5)P_3 generated by p110-β to produce PtdIns(3)P in the endosomal compartment (Shin et al., 2005). This mechanism would provide an alternate route for PtdIns(3)P production within the Vps34–Vps15–Beclin 1 complex that would require p110-β kinase activity. To test if p110-β kinase activity is

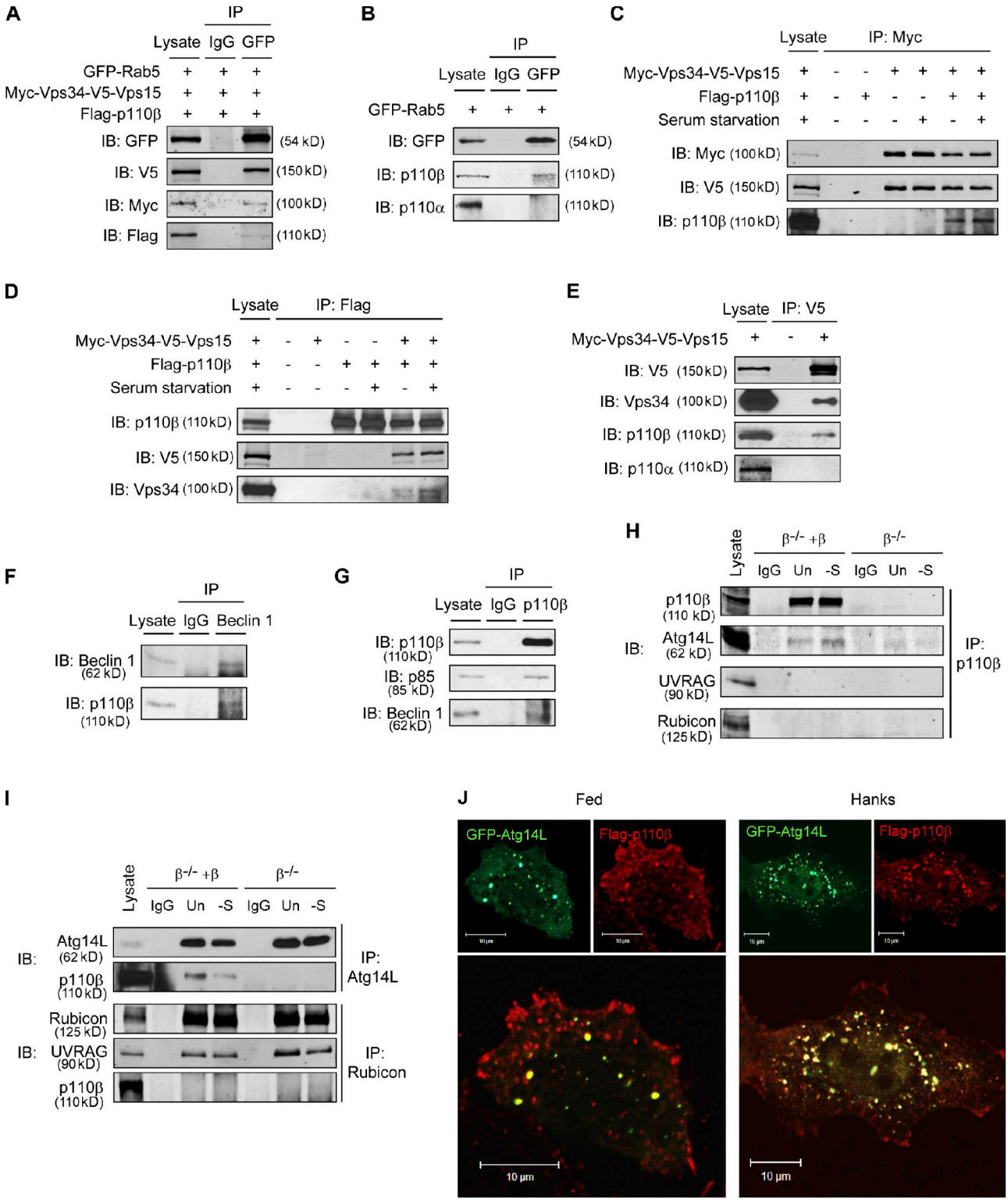

Figure 6. **p110-β is a component of the Vps34–Vps15–Beclin 1–Atg14L complex.** (A) HEK293T cells were transfected with indicated plasmids. Cell lysates were subjected to immunoprecipitation using IgG control or GFP antibody. The lysates and precipitates were analyzed with indicated antibodies. (B) GFP-Rab5–transfected HEK293T cells were subjected to immunoprecipitation, and the precipitates were immunoblotted with indicated antibodies. (C–E) HEK293T cells were transfected with indicated plasmids. Cells were either cultured in complete medium or in serum-free medium for 12 h. Cell extracts were made and subjected to immunoprecipitation using Myc, Flag, or V5 antibodies. The precipitates together with lysates were subjected to immunoblotting with indicated antibodies. (F and G) 293T (F) or MCF10A (G) cell lysates were subjected to immunoprecipitation using IgG, Beclin 1, or p110-β antibodies. The precipitates together with cell lysates were analyzed with indicated antibodies. (H and I) $\beta^{-/-}$ and p110-β–reconstituted $\beta^{-/-}$ MEFs were cultured in complete medium or in serum-free medium for 6 h. Cell extracts were subjected to immunoprecipitation using IgG control, p110-β antibody (H), or Atg14L and Rubicon antibodies (I). The precipitates and cell lysates were analyzed with indicated antibodies. (J) HeLa cells were transfected with Flag–p110-β together with GFP-Atg14L constructs. Cells were left untreated or starved in Hank's buffer for 4 h. The cells were fixed and stained with Flag and Alexa 594–conjugated antibodies, and observed under a confocal fluorescence microscope. Representative images with green, red, or merged channels are shown.

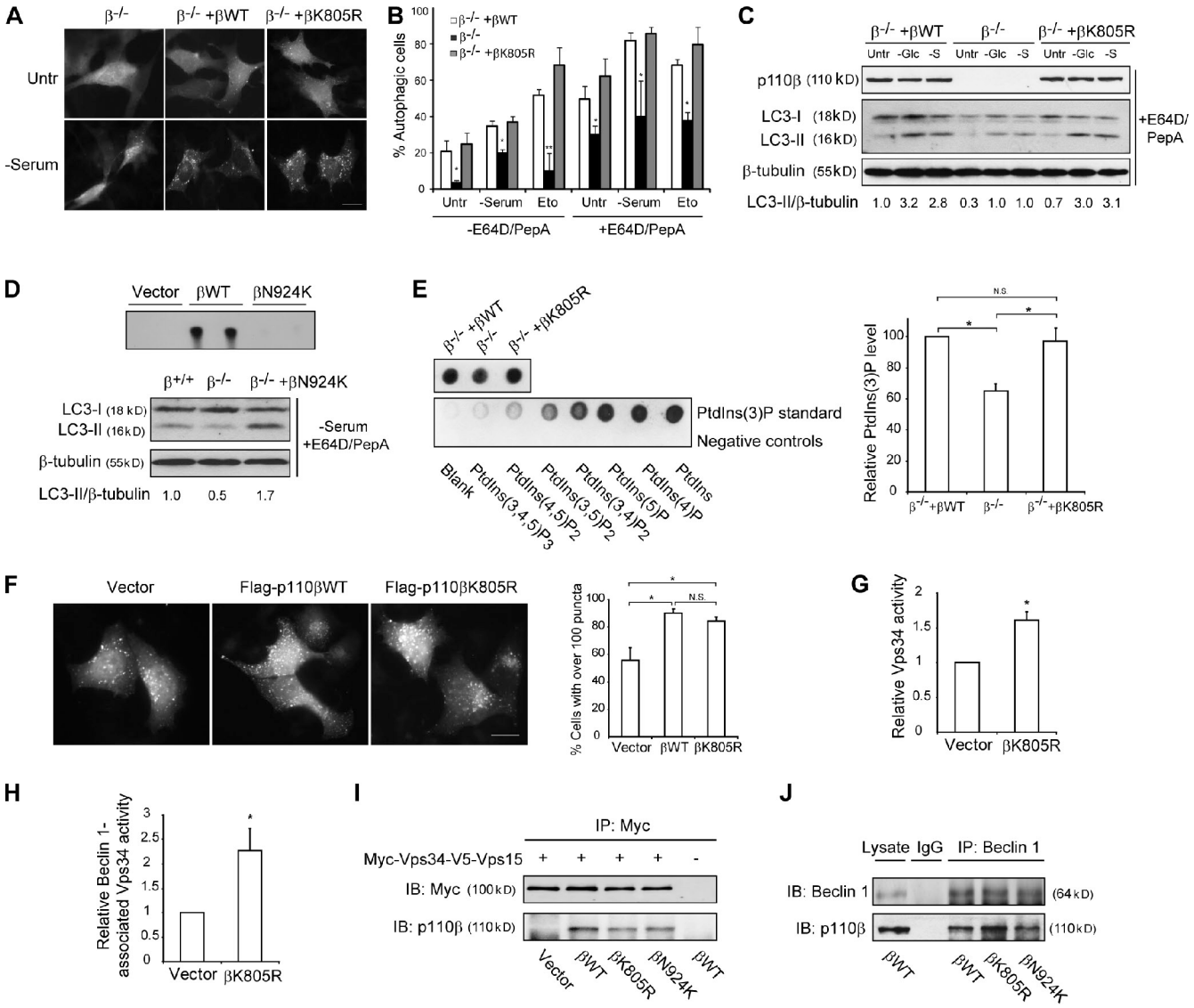

Figure 7. **p110-β promotes autophagy independently of its kinase activity.** (A) $\beta^{-/-}$ MEFs expressing GFP-LC3 were stably reconstituted with construct expressing p110-βWT or p110-βK805R mutant. Cells were left untreated or serum starved for 6 h. Cells were fixed and imaged under a deconvolution fluorescence microscope. Representative images are shown. Bar, 20 µm. (B) Quantification of autophagic cell percentage of GFP-LC3–expressing MEFs upon indicated treatments. Data shown are averages of five blind countings ± SD. *, $P < 0.05$; **, $P < 0.005$. (C) The three cell lines were cultured in complete medium, glucose-free medium (12 h), or serum-free medium (6 h) in the presence of E64D and PepA. Cell lysates were immunoblotted with indicated antibodies. Quantification of LC3-II/β-tubulin is shown at bottom. (D, top) HEK293 cells were transfected with empty vector, or constructs expressing Flag-tagged p110-βWT or p110-βN924K. p110-β PI3K activity was assayed in Flag-immunoprecipitates. Results show an autoradiograph from duplicate assays. (Bottom) $\beta^{+/+}$, $\beta^{-/-}$, and $\beta^{-/-}$ MEFs reconstituted with p110-βN924K mutant were cultured in serum-free medium for 6 h in the presence of E64D and PepA. Cell extracts were probed for LC3 and β-tubulin, and the ratio of LC3-II/β-tubulin is shown. (E) MEFs with indicated genotypes were subject to protein–lipid overlay analysis for PtdIns(3)P content. Quantification of total cellular PtdIns(3)P normalized against total protein is shown on the right. Data shown are the mean values from three independent experiments (*, $P < 0.05$; N.S., nonsignificant; error bars = SEM). (F) HeLa cells were transfected with GFP-FYVE, together with vector control, Flag–p110-βWT, or Flag–p110-βK805R construct. 48 h after transfection, cells were fixed and observed under a deconvolution fluorescence microscope. Bar, 20 µm. Cells with over 100 GFP puncta were quantified and presented. Data shown within each group are the average of at least five independent countings with over 200 cells. Error bars = SD. *, $P < 0.05$; N.S., nonsignificant. (G and H) HEK293T cells overexpressing Myc–Vps34–V5–Vps15, Beclin 1–GFP, together with vector control or Flag–p110-βK805R were subjected to immunoprecipitation using an anti-Myc antibody (G) or a GFP antibody (H). Vps34 activity was determined. Data presented are the average of three independent experiments; error bars = SEM. *, $P < 0.05$. (I) HEK293T cells were transfected with the Myc–Vps34–V5–Vps15 bicistronic plasmid, together with empty vector or constructs expressing wild-type or kinase-dead p110-β mutants. Cell lysates were subject to immunoprecipitation using an anti-Myc antibody. The precipitates were immunoblotted for Myc and p110-β. (J) HEK293T cells were transfected with constructs expressing wild-type or kinase-dead p110-β mutants. Cell lysates were subject to immunoprecipitation using IgG or Beclin 1 antibody. The precipitates were probed for Beclin 1 and p110-β.

required for autophagy, $\beta^{+/+}$ MEFs were treated with TGX-221, a selective p110-β kinase inhibitor. TGX-221 did not inhibit LC3 conversion in basal state or under glucose or serum deprivation conditions (Fig. 3 A), suggesting that p110-β promotes autophagy independently of its kinase activity. To further address the kinase dependency issue, we reconstituted $\beta^{-/-}$ MEFs with either wild-type p110-β or the kinase-dead p110-βK805R mutant. The p110-βK805R mutant showed similar capabilities

in restoring GFP-LC3 puncta formation as that of p110-βWT (Fig. 7, A and B). In addition, both p110-βWT and p110-βK805R restored LC3 conversion to a similar extent (Fig. 7 C). Another kinase-dead mutant, p110-βN924K (Ballou et al., 2007) (Fig. 7 D), also restored LC3 conversion in $\beta^{-/-}$ MEFs (Fig. 7 D). Expression of p110-βK805R also enhanced PtdIns(3)P production, as indicated by the lipid–protein overlay assay (Fig. 7 E), GFP-FYVE puncta formation (Fig. 7 F), and increased Vps34 kinase activity (Fig. 7, G and H). Similar to wild-type p110-β, both p110-βK805R and p110-βN924K were able to interact with Vps34 and Beclin 1 (Fig. 7, I and J). Taken together, these results strongly suggest that p110-β functions as a scaffold, within the Vps34–Vps15–Beclin 1 complex, to positively regulate Vps34 activity, PtdIns(3)P production, and autophagy.

Deficiency of p110-β results in impaired autophagy in vivo

To investigate the role of p110-β in regulating autophagy in vivo, we tested autophagy response in the liver and the heart. The liver is one of the best characterized organs where autophagy plays an important physiological role (Komatsu et al., 2005). Here, *p110-β*$^{flox/flox}$ mice were bred with albumin-*Cre* mice, in which expression of the Cre recombinase is under the control of the liver-specific albumin promoter resulting in deletion of floxed genes by 6 wk after birth (Postic and Magnuson, 2000). Successful deletion of p110-β was confirmed in 8-wk-old mice (unpublished data). Littermates with either *p110-β*$^{flox/flox}$; albumin-*Cre*$^{-}$ or *p110-β*$^{wt/wt}$; albumin-*Cre*$^{+}$ genotypes were used as controls for the possible effect of either floxed *p110-β* or Cre. Because no obvious differences between these two groups were observed, we refer to both control lines as $\beta^{+/+}$ and hereafter do not distinguish between them. Upon 24 h of fasting, protein content significantly decreased in $\beta^{+/+}$ livers, but fasting-induced liver protein degradation was suppressed in $\beta^{-/-}$ livers (Fig. 8 A). We did not observe an increase in protein content in $\beta^{-/-}$ livers under fed condition as that of *Atg7*$^{-/-}$ livers (Komatsu et al., 2005), most likely because p110-β is also required for normal growth. Indeed, the p110-β kinase–deficient mice showed severe growth retardation (Ciraolo et al., 2008). Compared with the $\beta^{+/+}$ liver, EM analysis revealed deformed mitochondria and deficient formation of hyaloplasmic glycogen areas in $\beta^{-/-}$ livers (Fig. 8 B), reminiscent of the autophagy-deficient *Atg7*$^{-/-}$ liver (Komatsu et al., 2005). After 24 h fasting, the $\beta^{+/+}$ liver showed accumulation of autophagosomes, whereas the $\beta^{-/-}$ liver did not (Fig. 8 B). Western blotting of liver lysates showed elevated levels of polyubiquitinated proteins and p62 in the $\beta^{-/-}$ liver (Fig. 8, C and D). To further study the involvement of p110-β in liver autophagy, *p110-β*$^{flox/flox}$ mice were bred with GFP-LC3 transgenic mice (Mizushima et al., 2004), then with the albumin-*Cre* mice. A 24-h fast resulted in the accumulation of GFP-LC3 puncta in the $\beta^{+/+}$ liver, whereas this response was markedly decreased in the $\beta^{-/-}$ liver (Fig. 8 E). Similarly, Beclin 1–GFP knock-in mice (Zhong et al., 2009) were bred with *p110-β*$^{flox/flox}$; albumin-*Cre* mice. Although a 24-h fast resulted in accumulation of Beclin 1–GFP puncta in the $\beta^{+/+}$ liver, this response was markedly impaired in the $\beta^{-/-}$ liver (Fig. S5), suggesting a defect in the early stage of autophagy. In addition to the liver, we investigated fasting-induced autophagy in the p110-$\beta^{-/-}$ heart. *p110-β*$^{flox/flox}$ mice were bred with MCK-*Cre* mice (Brüning et al., 1998) to delete p110-β in cardiac and skeletal muscles (unpublished data), then with GFP-LC3 mice. 48 h of fasting dramatically induced GFP-LC3 puncta in the $\beta^{+/+}$ heart, whereas it failed to do so in the $\beta^{-/-}$ heart (Fig. 8 F).

Besides starvation-induced autophagy, we also tested autophagy induced by pressure overload in the heart by TAC (Zhu et al., 2007). In this study, p110-β is deleted in the heart of adult MerCreMer; *p110-β*$^{flox/flox}$ mice by tamoxifen injection (Lu et al., 2009). As compared with the tamoxifen-injected littermate controls (do not express MerCreMer), the *p110-β*–deleted hearts displayed deficiency in autophagosome formation upon TAC (Fig. 9 A). In agreement with this observation, the MCK-*Cre*; GFP-LC3; *p110-β*$^{flox/flox}$ and their littermate control mice were also subjected to TAC. The procedure induced a marked increase in the number of GFP-LC3 puncta in $\beta^{+/+}$ hearts, whereas very few GFP-LC3 puncta were observed in $\beta^{-/-}$ hearts after TAC (Fig. 9 B). Taken together, these results indicate that p110-β is a positive regulator of autophagy in vivo.

Discussion

Class IA PI3Ks are critical regulators of a wide variety of cellular functions. Their most prominent biological activity is to activate the Akt–TOR signaling pathway via the generation of PtdIns(3,4,5)P_3 (Engelman et al., 2006). It is thus predicted that class IA PI3Ks should negatively regulate autophagy. However, the direct involvement of class IA PI3K in autophagy has not been addressed. Here, we provide evidence showing that the p110-β catalytic subunit, but not p110-α, can function as a positive regulator of autophagy. It promotes autophagy by facilitating PtdIns(3)P generation, possibly in the localized compartment together with the autophagy-essential Vps34–Vps15–Beclin 1–Atg14L complex (Fig. 10). This autophagy-promoting role of p110-β is not tissue specific, as compromised autophagy was observed in $\beta^{-/-}$ MEF, liver, and heart, and overexpression of p110-β resulted in enhanced autophagy in multiple cell lines.

Our observation does not contradict the role of the Akt–TOR pathway on autophagy regulation. Rather, we find that p110-β promotes autophagy independently of Akt–TOR signaling, and may be through the enhanced generation of cellular PtdIns(3)P. This theory would suggest that although p110-β is classified as a class IA PI3K, it can promote the generation of PtdIns(3)P, which is a well-recognized product of the class III PI3K Vps34. We find here that p110-β may act as a scaffold, independently of its kinase activity, within the Rab5–Vps34–Vps15–Beclin 1 complex to promote the catalytic activity of Vps34 (Figs. 4, 6, and 7). Indeed, the scaffold function of p110-β has been noticed. The kinase-deficient p110-β mutant was able to correct some defects of $\beta^{-/-}$ cells in cell growth, ribosomal protein S6 phosphorylation, endocytosis, and EEA1 endosomal recruitment (Ciraolo et al., 2008; Jia et al., 2008). The kinase-deficient p110-β knock-in rescued the embryonic lethality of $\beta^{-/-}$ mice (Ciraolo et al., 2008). In line with these studies, our findings not only uncover a novel function of p110-β, but also provide new insights into the biological relevance of its kinase-independent activity.

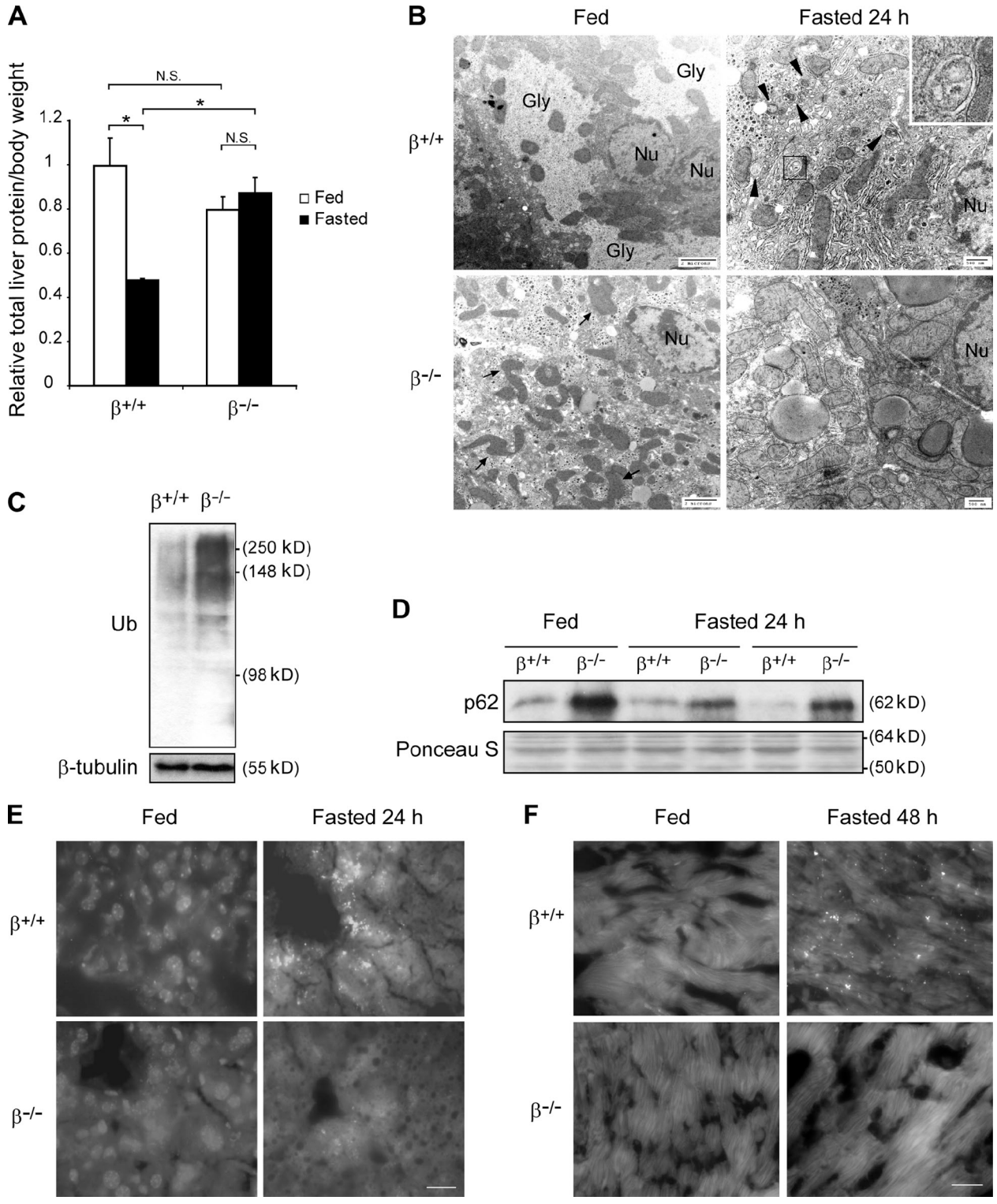

Figure 8. **Autophagy is impaired in p110-β-deficient liver and heart.** (A) Gender- and age-paired 8- to 10-wk-old mice with indicated genotypes were fed or fasted for 24 h. Liver weight, body weight, and liver protein concentrations were measured. Data presented are the normalized average values ± SEM; $n = 5$ within each group; *, $P < 0.05$; N.S., nonsignificant. (B) Electron micrographic images of livers from 8-wk-old fed or 24-h fasted mice. Deformed mitochondria are indicated by arrow in the $\beta^{-/-}$ liver. In fasted livers, autophagosomes are labeled with arrowheads. Higher magnification view of a representative autophagosome is shown in the inset. Note the swollen mitochondria in fasted $\beta^{-/-}$ liver. Gly, glycogen area; Nu, nucleus. (C) Total lysates were made from $\beta^{+/+}$ and $\beta^{-/-}$ livers, and probed for ubiquitin and β-tubulin. Data shown are representative of three independent pairs of animals. (D) Total liver lysates from fed or 24-h fasted mice with indicated genotypes were generated, and immunoblotted for p62. Ponceau S staining is shown for equal loading. (E) 8-wk-old GFP-LC3 transgenic mice with indicated liver genotypes were fed or fasted for 24 h. Cryosections of the livers were observed under a deconvolution fluorescence microscope. Representative images are shown. Bar, 20 µm. (F) GFP-LC3 transgenic mice with indicated heart genotypes were fed or fasted for 48 h. Heart cryosections were observed and representative images are shown. Bar, 20 µm. Note the increase in GFP-LC3 puncta in fasted $\beta^{+/+}$ liver and heart, which are impaired in fasted $\beta^{-/-}$ mice.

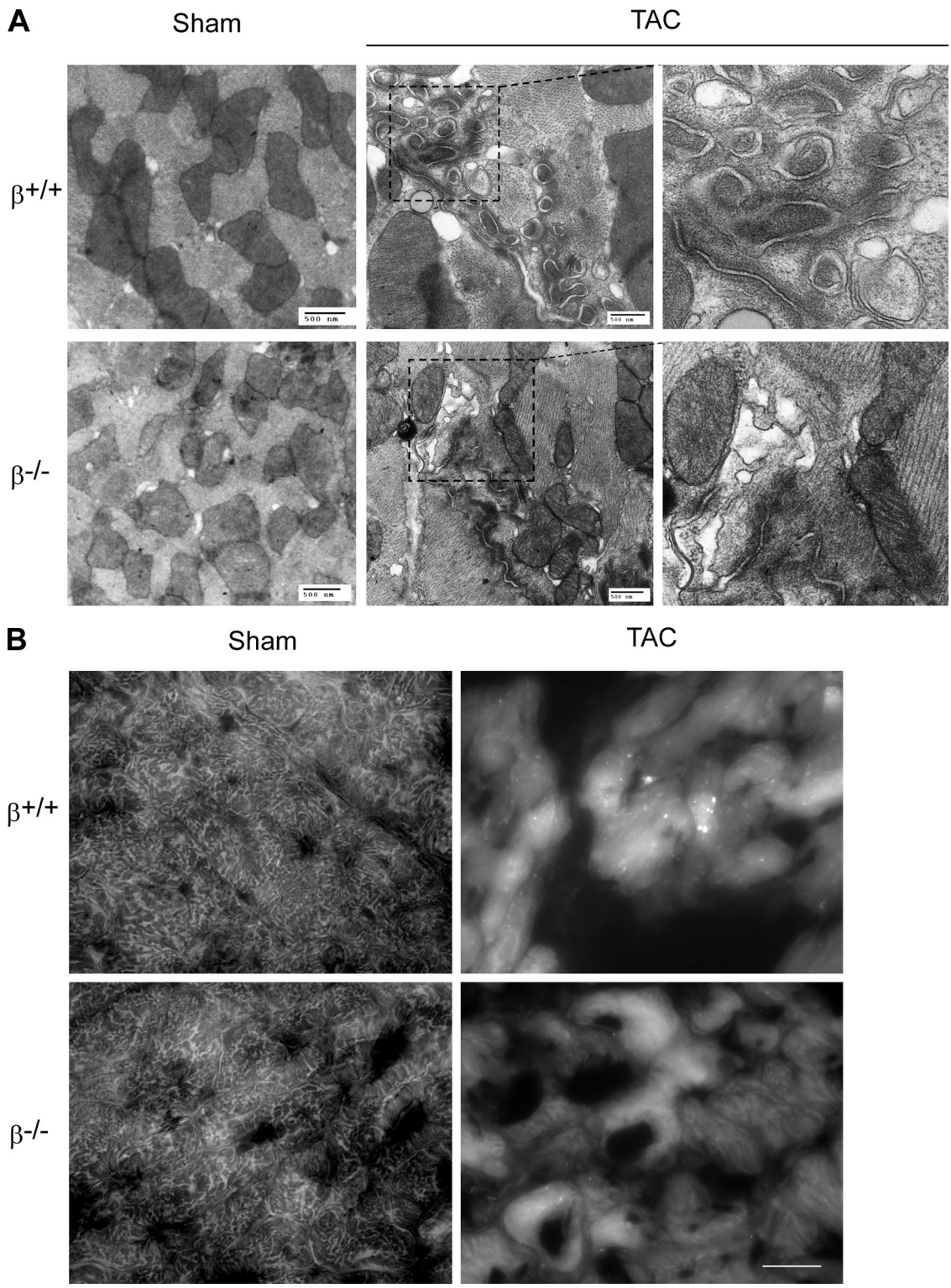

Figure 9. **p110-β is required for autophagy induced by pressure overload in the heart.** (A) At 8 wk of age, MerCreMer;*p110-β*$^{flox/flox}$ mice and their littermate *p110-β*$^{flox/flox}$ controls were injected with 1 mg tamoxifen intraperitoneally daily for 28 d. 4 wks later, transverse aortic constriction (TAC) or sham operation was performed on these tamoxifen-injected mice. 33 d later, hearts were harvested and sections were prepared for electron microscopy. Representative images are shown for each group of mice. Note the dramatic induction of autophagosomes in the $\beta^{+/+}$ heart, which is absent in the $\beta^{-/-}$ heart. (B) TAC or sham operation was performed on 10–12-wk-old MCK-*Cre*;GFP-LC3;*p110-β*$^{flox/flox}$ mice and their littermate GFP-LC3;*p110-β*$^{flox/flox}$ controls. 7 d later, hearts were harvested and frozen sections prepared. GFP-LC3 puncta in the heart sections were visualized under a deconvolution fluorescence microscope. Representative images with the same magnification are shown for each group of mice. Bar, 20 μm.

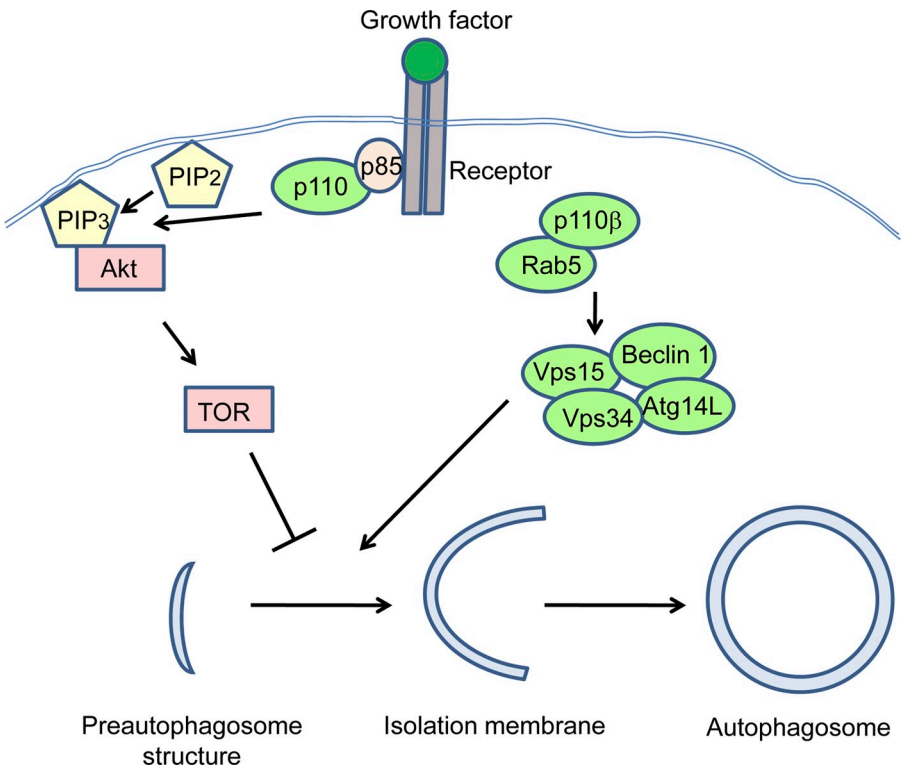

Figure 10. **Schematic model for p110-β in the regulation of autophagy.** Growth factors activate membrane receptors (such as RTK and GPCR), which recruit p85-p110 and stimulate the production of PtdIns(3,4,5)P_3, which in turn activates the Akt–TOR pathway and inhibits autophagy. On the other hand, p110-β (but not p110-α) localizes in the autophagy-promoting complex that contains Rab5, Vps34, Vps15, Beclin 1, and Atg14L. The complex produces PtdIns(3)P and facilitates the formation of autophagosomes.

Although our findings point to the importance of the scaffold function of p110-β, we cannot exclusively rule out the possibility that its kinase activity also contributes to promoting PtdIns(3)P generation and autophagy. In addition to transducing receptor signals by producing PtdIns(3,4,5)P_3, p110-β is also known to produce PtdIns(3)P in the Rab5-containing environment, by association with a protein complex containing PtdIns 4- and 5-phosphatases that dephosphorylate PtdIns(3,4,5)P_3 generated by p110-β (Shin et al., 2005). The currently recognized source of PtdIns(3)P for autophagy has been attributed to Vps34. However, a recent report shows that *vps34*$^{-/-}$ sensory neurons are defective in endolysosomal pathway although capable of autophagosome formation (Zhou et al., 2010). This suggests a Vps34-independent mechanism of PtdIns(3)P production, which may be fulfilled by other PI3Ks and phosphatases, including p110-β. Further studies, such as the generation of cells and/or animals doubly deficient in Vps34 and p110-β, will help to clarify this issue.

Our finding broadens the complexity of PI3K functions in metazoans. Yeast, a unicellular eukaryotic organism, only possesses the class III PI3K Vps34 that regulates membrane trafficking and autophagy (Engelman et al., 2006; Backer, 2008). In addition to evolutionarily conserved class III PI3K, class I PI3Ks that transduce signals from cell surface receptors and activate Akt–TOR pathways have evolved in multicellular organisms (Engelman et al., 2006). Among various p110 isoforms in metazoans, the ubiquitously expressed p110-α and -β isoforms share similar yet distinct roles. Although both isoforms respond to membrane receptor signals, the p110-α isoform is involved mostly in RTK-mediated Akt signaling, whereas p110-β has been found to have distinct activity in GPCR-mediated Akt activation (Zhao et al., 2006; Guillermet-Guibert et al., 2008; Jia et al., 2008). Together with previous reports, our observations suggest that while p110-β regulates receptor-mediated cell activation by producing PtdIns(3,4,5)P_3 as a lipid kinase, it can also promote endocytosis and autophagy as a scaffold-modulator of class III PI3K activity. Our results indicate that class I PI3Ks are not only mediators of cell activation, but are also critical regulators in maintaining cellular homeostasis. This provides additional evidence for the functional evolution of class I PI3Ks in metazoans. Our demonstration of an autophagy-promoting function of p110-β suggests a new perspective for understanding the physiological and pathological roles of PI3Ks in metabolism, tissue homeostasis, and cancer development.

Materials and methods

Mice

p110-α$^{+/+}$, p110-α$^{-/-}$, p110-β$^{+/+}$, and p110-β$^{-/-}$ mice were described previously (Lu et al., 2009). Beclin 1–EGFP knock-in mice were described elsewhere (Zhong et al., 2009). GFP-LC3 transgenic mice (Mizushima et al., 2004) were gifts from Dr. Noboru Mizushima (Tokyo Medical and Dental University, Tokyo, Japan). Albumin-Cre mice were purchased from The Jackson Laboratory. For fasting studies, mice were deprived of food while having free access to water. All mice were experimented in compliance with the Stony Brook University Institutional Animal Care and Use Committee guidelines.

Cell lines, culture, and transfection

Primary mouse embryonic fibroblasts (MEFs) were generated from d 14–17 embryos from p110-α (flox$^{+/-}$) or p110-β (flox$^{+/-}$) matings (Lu et al., 2009). Early passage MEFs were immortalized by transfection of SV40 large T antigen–encoding plasmid. Immortalized MEFs were infected with either adenoviral GFP to generate α$^{+/+}$ or β$^{+/+}$ MEFs, or adenoviral Cre-GFP to generate α$^{-/-}$ or β$^{-/-}$ MEFs.

MEFs, HEK293, 293T, BMK, and HeLa cells were cultured in DME supplemented with 10% fetal bovine serum (FBS), 100 units/ml penicillin,

and 100 µg/ml streptomycin (Invitrogen), and transfected by Lipofectamine 2000 (Invitrogen). MCF10A cells were cultured in DME/F12 (Invitrogen) supplemented with 5% horse serum (Invitrogen), 20 ng/ml EGF (Sigma-Aldrich), 0.5 mg/ml hydrocortisone (Sigma-Aldrich), 100 ng/ml cholera toxin (Sigma-Aldrich), 10 µg/ml insulin (Sigma-Aldrich), 100 units/ml penicillin, and 100 µg/ml streptomycin.

Plasmids

GFP-LC3 constructs were described previously (Ullman et al., 2008). The bicistronic Myc–Vps34–V5–Vps15 (Yan et al., 2009) is a gift from Dr. Jonathan Backer (Albert Einstein College of Medicine, Bronx, NY). Beclin 1–GFP and GFP-Atg14L have been described previously (Zhong et al., 2009). GFP-DFCP1 is a gift from Dr. Nicholas Ktistakis (Babraham Institute, Cambridge, UK; Axe et al., 2008). mCherry–GFP-LC3 is a gift from Dr. Terje Johanson (University of Tromsø, Tromsø, Norway; Pankiv et al., 2007). CMV 3×Flag constructs expressing Flag–p110-β have been described previously (Ballou et al., 2007). The retroviral LPC–p110-β was generated by cloning the p110-β fragment from CMV 3×Flag–p110-β into retroviral LPC vector. GFP-FYVE and GFP-Rab5 constructs are gifts from Dr. Deborah Brown (Stony Brook University, Stony Brook, NY).

Reagents and antibodies

DME, glucose-free DME, Hank's buffer, and LysoTracker red were purchased from Invitrogen; tunicamycin, E64D (used at 10 µg/ml), Akt inhibitor (Akti) from EMD; pepstatin A (used at 10 µg/ml), rapamycin, Ponceau S, and 3-methyladenine (3-MA, used at 1 mM) from Sigma-Aldrich; and etoposide from Takara Bio Inc. TGX-221 was described previously (Lu et al., 2009). The reagent concentrations are indicated in figure legends.

The following antibodies were used: rabbit polyclonal GFP, Atg14L, and Rubicon (Zhong et al., 2009). Phosphotyrosine peptide-conjugated agarose, p85, p110-α, and p110-β antibodies were described previously (Lu et al., 2009). The following antibodies were purchased commercially: p110-β (1:1,000 for WB, 1:50 for IP; Cell Signaling Technology), p62/SQSTM1 (1:100,000; Abnova), LC3 (1:500, Novus Biologicals; 1:500, Cell Signaling Technology; and 1:1,000, MBL), ubiquitin (1:1,000, P4D1; Covance), β-tubulin (1:2,000; Sigma-Aldrich), Vps34 (1:250, Echelon Biosciences; 1:250, Cell Signaling Technology), GFP (1:5,000; Santa Cruz Biotechnology, Inc.), Myc (9E10, 1:500 for WB; Invitrogen), V5 (1:4,000 for WB, 1 µg/ml for IP; Invitrogen), Beclin 1 (1:1,000 for WB and 1 to 2 µg/ml for IP; Santa Cruz Biotechnology, Inc.), rabbit IgG (American Qualex), p-Akt 308 and 473 (1:1,000; Cell Signaling Technology), Flag (M2, 1:2,000 for WB and 1:150 for IF; Sigma-Aldrich), Atg5 (1:500; Abgent), UVRAG (1:1,000; MBL), PtdIns(3)P (Echelon Biosciences), PtdIns(3,4,5)P_3 (Echelon Biosciences), and Alexa 594–conjugated anti–mouse secondary antibody (1:500 for IF; Invitrogen).

Retroviral and lentiviral infection

Stable cell lines were generated by retroviral infection. Retrovirus infection was performed as described previously (Ullman et al., 2008). The lentiviral sh–p110-β construct was purchased from Sigma-Aldrich. 5×10^5 HEK293T cells were plated into a 6-well plate. After overnight recovery, cells were transfected with LPC-retroviral constructs together with helper virus construct, or lentiviral constructs and packaging plasmids. 24 h after transfection, the supernatant containing viral particles was supplemented with 10 µg/ml polybrene (Sigma-Aldrich), and filtered through a 0.45-µm filter. The supernatant was incubated with recipient cells in a 6-well plate. Infections were repeated twice, at 12- and 24-h intervals. For retrovirus-generated stable cell lines, 3 d after the first infection, infected recipient cells were selected with puromycin (InvivoGen).

Electron microscopy

Samples were processed as described previously (Guerriero et al., 2008; Ullman et al., 2008), with slight modification. Tissue samples were collected freshly and fixed in 4.0% PFA, 2.5% EM grade glutaraldehyde in 0.1 M PBS, pH 7.4. Cell samples were fixed in 2.5% EM-grade glutaraldehyde in 0.1 M PBS, pH 7.4. After fixation, samples were placed in 2% osmium tetroxide for tissues and 1% for cells in 0.1 M PBS, pH 7.4, dehydrated in a graded series of ethyl alcohol, and embedded in epon resin for tissues and Durcupan resin for cells. Ultra-thin sections of 80 nm were cut with an ultramicrotome (UltracutE; Reichert-Jung) and placed on formvar-coated slot copper grids. Sections were counterstained with uranyl acetate and lead citrate, and viewed with an electron microscope (Tecnai12 BioTwinG2; FEI). Images were acquired with a CCD digital camera system (model XR-60; Advanced Microscopy Techniques Corp.).

GFP-LC3 puncta observation and quantification

Quantification of GFP-LC3 was performed as described previously (Ullman et al., 2008). In brief, cells expressing GFP-LC3 were treated and fixed in 4% PFA in PBS and observed under an inverted microscope (Axiovert 200M; Carl Zeiss, Inc.) using the 63× oil objective. 50–200 cells were randomly selected and counted for autophagy induction. The cells with more than 10 green puncta and less nuclear GFP signal were considered autophagic. Quantification was performed independently by Z. Dou and J.-A. Pan.

For cryosections, the tissue was embedded directly in Optimal Cutting Temperature Compound (Sakura), stored at −80°C, and sectioned into 6-µm sections. GFP-LC3 and Beclin 1–GFP puncta were observed and imaged under an inverted microscope (Axiovert 200M; Carl Zeiss, Inc.) using the 63× oil objective.

Measurement of long-lived protein degradation

MEFs (10^5) were plated into a 12-well plate. After overnight recovery, the cells were labeled with 0.5 µCi/ml ^{14}C-L-valine in L-valine–free medium (Invitrogen). 24 h after labeling, cells were washed three times with PBS, and incubated in complete medium plus 10 mM unlabeled L-valine for 24 h to chase out short-lived proteins. The cells were washed again for three times with PBS, and cultured either in complete medium or in serum-free medium, both containing 10 mM unlabeled L-valine. The supernatant was taken at indicated time points, and precipitated with ice-cold trichloroacetic acid (TCA) at a final concentration of 10%. The TCA-soluble radioactivity was measured by liquid scintillation counting. At the end of the experiments, cells were precipitated with 10% ice-cold TCA, washed with 10% TCA, and dissolved in 0.2 N NaOH, and the radioactivity was measured. The degradation of long-lived protein was calculated by the radioactivity in TCA-soluble supernatant normalized against the total ^{14}C-radioactivity present in supernatants and cell pellets.

Flow cytometry

For PtdIns(3)P and PtdIns(3,4,5)P_3 flow cytometry analysis, 10^6 MEFs were washed with FACS buffer (PBS with 1.5% FBS) and fixed in 100 µl 1% PFA in PBS for 10 min at room temperature. After incubation with 0.03% saponin in PBS, cells were incubated with primary antibodies diluted in PBS with 0.3% saponin and 20% goat serum, for 30 min at 4°C. After another wash with 0.03% saponin in PBS, fluorophore-conjugated secondary antibodies were added to samples for 30 min at 4°C. The cells were washed twice with 0.03% saponin in PBS, once with FACS buffer, and resuspended in 0.5 ml FACS buffer. The samples were analyzed using a flow cytometer (FACSCalibur; BD).

Protein–lipid overlay assay

Total cellular PtdIns(3)P measurement was performed using the PI(3)P Mass Strip kit (Echelon Biosciences). MEFs with ∼80% confluency in 10-cm plates were harvested by trypsinization. 5–10% of the total cells were lysed, and the protein concentration determined by the BCA Protein Assay kit (Thermo Fisher Scientific). Cells with equal amounts of total protein were subjected to lipid extraction and protein–lipid overlay analysis following the manufacturer's protocol. PtdIns(3)P samples and standards were visualized by ECL (Thermo Fisher Scientific) and quantified by ImageJ software (NIH, Bethesda, MD).

Immunoprecipitation

Cells were lysed with lysis buffer (20 mM Tris, pH 7.5, 137 mM NaCl, 1 mM $MgCl_2$, 1 mM $CaCl_2$, 100 mM NaF, 10 mM sodium pyrophosphate, 100 µM orthovanadate, 1% NP-40, 10% glycerol, and 200 µM PMSF) supplemented with protease inhibitor complex (Roche). Cell lysates were centrifuged at 17,000 *g* for 10 min; 500 µg to 1 mg of soluble protein was incubated with primary antibodies overnight at 4°C, with concentrations described in the Reagents and antibodies section. Protein A– or G–agarose (Roche) was added and incubated at 4°C for 1 h. The Myc and Flag immunoprecipitations were performed using anti-Myc or anti-Flag antibody-conjugated agarose (Sigma-Aldrich) following the manufacturer's protocols. The precipitates were then washed 4–5 times with lysis buffer, boiled with 1× protein loading dye, and subjected to Western blotting.

Immunofluorescence

Cells were fixed in 4% paraformaldehyde (PFA) in PBS for 20 min at room temperature. Cells were washed twice with PBS, and permeabilized with 0.1% Triton X-100 in PBS for 10 min. After washing two times, cells were blocked in 5% goat serum in PBS overnight at 4°C. Primary antibodies were incubated with 5% goat serum in PBS overnight at 4°C. Cells were washed four times with PBS containing 0.1% Tween 20 (PBST), followed by

incubation with fluorophore-conjugated secondary antibody in 5% goat serum in PBST for 1 h at room temperature. Cells were then washed four times in PBST, and incubated with 1 µg/ml DAPI in PBS for 5 min. Cells were washed twice with PBS, and mounted with Immu-Mount (Thermo Fisher Scientific). The slides were observed and imaged using a two-photon laser scanning confocal microscope (LSM 510 META NLO; Carl Zeiss, Inc.), or an inverted microscope (Axiovert 200M; Carl Zeiss, Inc.).

PI3K activity assays

For Vps34 kinase assays, HEK293T cells were transfected with indicated plasmids. 48 h after transfection, cells were harvested, and cell pellets were washed with 5 ml ice-cold PBS and 5 ml ice-cold wash buffer (20 mM Tris, pH 7.5, 137 mM NaCl, 1 mM $MgCl_2$, 1 mM $CaCl_2$, 100 mM sodium fluoride, and 10 mM sodium pyrophosphate). Vps34 activity lysis buffer (20 mM Tris, pH 7.5, 137 mM NaCl, 1 mM $MgCl_2$, 1 mM $CaCl_2$, 100 mM sodium fluoride, 10 mM sodium pyrophosphate, 100 µM orthovanadate, 1% NP-40, 10% glycerol, and 200 µM PMSF) was added and the cells were kept on ice for 10 min with frequent vortexing, followed by centrifugation at 18,000 *g* for 10 min at 4°C. Protein concentration of the supernatant was determined by Bradford assays (Bio-Rad Laboratories). Equal amounts of supernatant protein were gently mixed at 4°C overnight with Myc antibody-conjugated agarose (Invitrogen) or rabbit polyclonal GFP antibody. Protein A–agarose was added to GFP antibody-containing samples with further mixing for 2 h at 4°C. The beads were washed three times with 1 ml of lysis buffer for 5 min at 4°C, followed by two washes with 1 ml of Vps34 assay buffer (50 mM Hepeps, pH 7.5, 100 mM NaCl, 2 mM dithiothreitol, and 1 mM EGTA) without dithiothreitol. 75% of the beads were suspended in 40 µl of Vps34 assay buffer. Kinase assays were started by adding 5 µl of 2 mg/ml L-α-phosphatidylinositol (Sigma-Aldrich) sonicated in Vps34 assay buffer and 5 µl of reaction mix containing 400 µM ATP, 50 mM $MnCl_2$, and 0.25 µl of γ-[^{32}P]ATP (3,000 Ci/mmol; PerkinElmer) per assay in Vps34 assay buffer. Tubes were heated at 30°C for 15 min with shaking. The reactions were stopped with 120 µl of $CHCl_3$/CH_3OH/HCl (10:20:0.2) and the tubes were put on a shaker for 10 min. After centrifuging for 5 min, 15 µl of the lower phase was spotted onto a silica gel thin-layer plate, and the reaction product was separated by chromatography for 1.5 h in $CHCl_3$/CH_3OH/NH_4OH/H_2O (86:76:10:14). Radioactive spots containing PtdIns(3)P were visualized by autoradiography, cut out of the plate, and quantified by scintillation counting. The other 25% of beads were boiled in SDS sample buffer and subjected to immunoblotting. Signals were quantified using the Odyssey Infrared Imaging System (LI-COR Biosciences). Vps34 activity was calculated as cpm normalized to the amount of Vps34 immunoprecipitated.

For p110-β kinase assays, recombinant p110-β/p85α protein (Millipore) in 40 µl of PI3K assay buffer (20 mM Hepes, pH 7.5, 100 mM NaCl, and 0.5 mM EGTA) was mixed with 5 µl of 10 mg/ml L-α-phosphatidylinositol sonicated in PI3K assay buffer and 5 µl of reaction mix containing 400 µM ATP, 100 mM $MgCl_2$, and 0.25 µl of γ-[^{32}P]ATP per assay in PI3K assay buffer. Tubes were heated at 25°C for 20 min with shaking. The reactions were stopped and reaction products were analyzed as described above.

Transverse aortic constriction

Mice were anesthetized with 80 mg/kg ketamine and 10 mg/kg xylazine given intraperitoneally. The skin was cleaned with an iodine solution, and the operation was performed under sterile conditions. The surgical procedure was performed as described previously (Hu et al., 2003) with modifications. In brief, mice were placed in a supine position and a horizontal skin incision ~1.0 cm in length was made at the level of the suprasternal notch. A 3–5-mm longitudinal cut was made in the proximal portion of the sternum. This allowed visualization of the aortic arch under low-power magnification. A wire with a snare on the end was passed under the aorta between the origin of the right innominate and left common carotid arteries. A 6-0 silk suture was snared with the wire and pulled back around the aorta. A bent 27-gauge needle was then placed next to the aortic arch, and the suture was snugly tied around the needle and the aorta. After ligation, the needle was quickly removed and the skin was closed. The sham procedure was identical except that the aorta was not ligated.

Statistics

Student's *t* test was used to compare the differences between two groups. For comparison between more than two groups, one-way ANOVA with Tukey's post-hoc test was used. Significance was judged when $P < 0.05$.

Image processing and densitometry measurement

Images taken from deconvolution and confocal microscopes were viewed and processed by AxioVision LE and Zeiss LSM image browser, respectively. Images were processed in Adobe Photoshop to enhance the brightness and contrast. Densitometry of immunoblot bands was determined by ImageJ software, unless otherwise indicated.

Online supplemental material

Fig. S1 shows the validation of p110-$\alpha^{-/-}$ and p110-$\beta^{-/-}$ MEFs. Fig. S2 shows that p110-β positively regulates autophagy in HEK293 cells. Fig. S3 shows that autophagy is not impaired in p110-$\alpha^{-/-}$ MEFs. Fig. S4 shows that p110-β does not affect the steady-state levels of several key autophagy proteins, but is required for the early stage of autophagosome formation. Fig. S5 shows that p110-β is essential for starvation-induced Beclin 1 puncta in the liver. Online supplemental material is available at http://www.jcb.org/cgi/content/full/jcb.201006056/DC1.

We thank Drs. Noboru Mizushima, Jonathan Backer, Jianhua Zhang, Nicholas Ktistakis, Qingjun Wang, Howard Crawford, Deborah Brown, and Michael Frohman for reagents and suggestions. We thank Elzbieta Selinger, Juei-Suei Chen, Shengnan Liu, Namratha Sheshadri, Yongjun Fan, Chia-Yen Wu, Erica Ullman, Joseph Catanzaro, and Drs. Yun Zhong and Zhuo Zhou for technical assistance. We thank Susan Van Horn and Dr. Guowei Tian for assistance on TEM and fluorescence microscopy, respectively.

This work is supported by the National Institutes of Health (grants DK62722 and CA136754 to R.Z. Lin; and CA098092 and CA129536 to W.-X. Zong), Susan Komen for the Cure (grant KG081538 to W.-X. Zong), and the Carol Baldwin Breast Cancer Research Foundation (to W.-X. Zong).

Submitted: 9 June 2010
Accepted: 18 October 2010

References

Axe, E.L., S.A. Walker, M. Manifava, P. Chandra, H.L. Roderick, A. Habermann, G. Griffiths, and N.T. Ktistakis. 2008. Autophagosome formation from membrane compartments enriched in phosphatidylinositol 3-phosphate and dynamically connected to the endoplasmic reticulum. *J. Cell Biol.* 182:685–701. doi:10.1083/jcb.200803137

Backer, J.M. 2008. The regulation and function of Class III PI3Ks: novel roles for Vps34. *Biochem. J.* 410:1–17. doi:10.1042/BJ20071427

Ballou, L.M., E.S. Selinger, J.Y. Choi, D.G. Drueckhammer, and R.Z. Lin. 2007. Inhibition of mammalian target of rapamycin signaling by 2-(morpholin-1-yl)pyrimido[2,1-alpha]isoquinolin-4-one. *J. Biol. Chem.* 282:24463–24470. doi:10.1074/jbc.M704741200

Brüning, J.C., M.D. Michael, J.N. Winnay, T. Hayashi, D. Hörsch, D. Accili, L.J. Goodyear, and C.R. Kahn. 1998. A muscle-specific insulin receptor knockout exhibits features of the metabolic syndrome of NIDDM without altering glucose tolerance. *Mol. Cell.* 2:559–569. doi:10.1016/S1097-2765(00)80155-0

Burman, C., and N.T. Ktistakis. 2010. Regulation of autophagy by phosphatidylinositol 3-phosphate. *FEBS Lett.* 584:1302–1312. doi:10.1016/j.febslet.2010.01.011

Cantley, L.C. 2002. The phosphoinositide 3-kinase pathway. *Science.* 296:1655–1657. doi:10.1126/science.296.5573.1655

Chang, Y.Y., G. Juhász, P. Goraksha-Hicks, A.M. Arsham, D.R. Mallin, L.K. Muller, and T.P. Neufeld. 2009. Nutrient-dependent regulation of autophagy through the target of rapamycin pathway. *Biochem. Soc. Trans.* 37:232–236. doi:10.1042/BST0370232

Christoforidis, S., M. Miaczynska, K. Ashman, M. Wilm, L. Zhao, S.C. Yip, M.D. Waterfield, J.M. Backer, and M. Zerial. 1999. Phosphatidylinositol-3-OH kinases are Rab5 effectors. *Nat. Cell Biol.* 1:249–252. doi:10.1038/12075

Ciraolo, E., M. Iezzi, R. Marone, S. Marengo, C. Curcio, C. Costa, O. Azzolino, C. Gonella, C. Rubinetto, H. Wu, et al. 2008. Phosphoinositide 3-kinase p110beta activity: key role in metabolism and mammary gland cancer but not development. *Sci. Signal.* 1:ra3. doi:10.1126/scisignal.1161577

Domin, J., and M.D. Waterfield. 1997. Using structure to define the function of phosphoinositide 3-kinase family members. *FEBS Lett.* 410:91–95. doi:10.1016/S0014-5793(97)00617-0

Engelman, J.A., J. Luo, and L.C. Cantley. 2006. The evolution of phosphatidylinositol 3-kinases as regulators of growth and metabolism. *Nat. Rev. Genet.* 7:606–619. doi:10.1038/nrg1879

Fruman, D.A., R.E. Meyers, and L.C. Cantley. 1998. Phosphoinositide kinases. *Annu. Rev. Biochem.* 67:481–507. doi:10.1146/annurev.biochem.67.1.481

Guerriero, J.L., D. Ditsworth, Y.J. Fan, F.P. Zhao, H.C. Crawford, and W.X. Zong. 2008. Chemotherapy induces tumor clearance independent of apoptosis. *Cancer Res.* 68:9595–9600. doi:10.1158/0008-5472.CAN-08-2452

Guillermet-Guibert, J., K. Bjorklof, A. Salpekar, C. Gonella, F. Ramadani, A. Bilancio, S. Meek, A.J.H. Smith, K. Okkenhaug, and B. Vanhaesebroeck. 2008. The p110beta isoform of phosphoinositide 3-kinase signals downstream of G protein-coupled receptors and is functionally redundant with p110gamma. *Proc. Natl. Acad. Sci. USA.* 105:8292–8297. doi:10.1073/pnas.0707761105

Hawkins, P.T., K.E. Anderson, K. Davidson, and L.R. Stephens. 2006. Signalling through Class I PI3Ks in mammalian cells. *Biochem. Soc. Trans.* 34:647–662. doi:10.1042/BST0340647

Hu, P., D. Zhang, L. Swenson, G. Chakrabarti, E.D. Abel, and S.E. Litwin. 2003. Minimally invasive aortic banding in mice: effects of altered cardiomyocyte insulin signaling during pressure overload. *Am. J. Physiol. Heart Circ. Physiol.* 285:H1261–H1269.

Jia, S.D., Z.N. Liu, S. Zhang, P.X. Liu, L. Zhang, S.H. Lee, J. Zhang, S. Signoretti, M. Loda, T.M. Roberts, and J.J. Zhao. 2008. Essential roles of PI(3)K-p110beta in cell growth, metabolism and tumorigenesis. *Nature.* 454:776–779.

Juhász, G., J.H. Hill, Y. Yan, M. Sass, E.H. Baehrecke, J.M. Backer, and T.P. Neufeld. 2008. The class III PI(3)K Vps34 promotes autophagy and endocytosis but not TOR signaling in Drosophila. *J. Cell Biol.* 181:655–666. doi:10.1083/jcb.200712051

Kabeya, Y., N. Mizushima, T. Ueno, A. Yamamoto, T. Kirisako, T. Noda, E. Kominami, Y. Ohsumi, and T. Yoshimori. 2000. LC3, a mammalian homologue of yeast Apg8p, is localized in autophagosome membranes after processing. *EMBO J.* 19:5720–5728. doi:10.1093/emboj/19.21.5720

Kihara, A., Y. Kabeya, Y. Ohsumi, and T. Yoshimori. 2001. Beclin-phosphatidylinositol 3-kinase complex functions at the trans-Golgi network. *EMBO Rep.* 2:330–335. doi:10.1093/embo-reports/kve061

Klionsky, D.J., H. Abeliovich, P. Agostinis, D.K. Agrawal, G. Aliev, D.S. Askew, M. Baba, E.H. Baehrecke, B.A. Bahr, A. Ballabio, et al. 2008. Guidelines for the use and interpretation of assays for monitoring autophagy in higher eukaryotes. *Autophagy.* 4:151–175.

Komatsu, M., S. Waguri, T. Ueno, J. Iwata, S. Murata, I. Tanida, J. Ezaki, N. Mizushima, Y. Ohsumi, Y. Uchiyama, et al. 2005. Impairment of starvation-induced and constitutive autophagy in Atg7-deficient mice. *J. Cell Biol.* 169:425–434. doi:10.1083/jcb.200412022

Kraft, C., A. Deplazes, M. Sohrmann, and M. Peter. 2008. Mature ribosomes are selectively degraded upon starvation by an autophagy pathway requiring the Ubp3p/Bre5p ubiquitin protease. *Nat. Cell Biol.* 10:602–610. doi:10.1038/ncb1723

Kundu, M., T. Lindsten, C.Y. Yang, J.M. Wu, F.P. Zhao, J. Zhang, M.A. Selak, P.A. Ney, and C.B. Thompson. 2008. Ulk1 plays a critical role in the autophagic clearance of mitochondria and ribosomes during reticulocyte maturation. *Blood.* 112:1493–1502. doi:10.1182/blood-2008-02-137398

Levine, B., and G. Kroemer. 2008. Autophagy in the pathogenesis of disease. *Cell.* 132:27–42. doi:10.1016/j.cell.2007.12.018

Levine, B., and J. Yuan. 2005. Autophagy in cell death: an innocent convict? *J. Clin. Invest.* 115:2679–2688. doi:10.1172/JCI26390

Liang, C., J.S. Lee, K.S. Inn, M.U. Gack, Q. Li, E.A. Roberts, I. Vergne, V. Deretic, P. Feng, C. Akazawa, and J.U. Jung. 2008. Beclin1-binding UVRAG targets the class C Vps complex to coordinate autophagosome maturation and endocytic trafficking. *Nat. Cell Biol.* 10:776–787. doi:10.1038/ncb1740

Lindmo, K., and H. Stenmark. 2006. Regulation of membrane traffic by phosphoinositide 3-kinases. *J. Cell Sci.* 119:605–614. doi:10.1242/jcs.02855

Lu, Z.J., Y.P. Jiang, W. Wang, X.H. Xu, R.T. Mathias, E. Entcheva, L.M. Ballou, I.S. Cohen, and R.Z. Lin. 2009. Loss of cardiac phosphoinositide 3-kinase p110 alpha results in contractile dysfunction. *Circulation.* 120:318–325. doi:10.1161/CIRCULATIONAHA.109.873380

Lum, J.J., R.J. DeBerardinis, and C.B. Thompson. 2005. Autophagy in metazoans: cell survival in the land of plenty. *Nat. Rev. Mol. Cell Biol.* 6:439–448. doi:10.1038/nrm1660

Matsunaga, K., T. Saitoh, K. Tabata, H. Omori, T. Satoh, N. Kurotori, I. Maejima, K. Shirahama-Noda, T. Ichimura, T. Isobe, et al. 2009. Two Beclin 1-binding proteins, Atg14L and Rubicon, reciprocally regulate autophagy at different stages. *Nat. Cell Biol.* 11:385–396. doi:10.1038/ncb1846

Mizushima, N., A. Yamamoto, M. Matsui, T. Yoshimori, and Y. Ohsumi. 2004. In vivo analysis of autophagy in response to nutrient starvation using transgenic mice expressing a fluorescent autophagosome marker. *Mol. Biol. Cell.* 15:1101–1111. doi:10.1091/mbc.E03-09-0704

Mizushima, N., B. Levine, A.M. Cuervo, and D.J. Klionsky. 2008. Autophagy fights disease through cellular self-digestion. *Nature.* 451:1069–1075. doi:10.1038/nature06639

Mizushima, N., T. Yoshimori, and B. Levine. 2010. Methods in mammalian autophagy research. *Cell.* 140:313–326. doi:10.1016/j.cell.2010.01.028

Pankiv, S., T.H. Clausen, T. Lamark, A. Brech, J.A. Bruun, H. Outzen, A. Øvervatn, G. Bjørkøy, and T. Johansen. 2007. p62/SQSTM1 binds directly to Atg8/LC3 to facilitate degradation of ubiquitinated protein aggregates by autophagy. *J. Biol. Chem.* 282:24131–24145. doi:10.1074/jbc.M702824200

Petiot, A., E. Ogier-Denis, E.F.C. Blommaart, A.J. Meijer, and P. Codogno. 2000. Distinct classes of phosphatidylinositol 3′-kinases are involved in signaling pathways that control macroautophagy in HT-29 cells. *J. Biol. Chem.* 275:992–998. doi:10.1074/jbc.275.2.992

Polson, H.E., J. de Lartigue, D.J. Rigden, M. Reedijk, S. Urbe, M.J. Clague, and S.A. Tooze. 2010. Mammalian Atg18 (WIPI2) localizes to omegasome-anchored phagophores and positively regulates LC3 lipidation. *Autophagy.* 6:506–522. doi:10.4161/auto.6.4.11863

Postic, C., and M.A. Magnuson. 2000. DNA excision in liver by an albumin-Cre transgene occurs progressively with age. *Genesis.* 26:149–150. doi:10.1002/(SICI)1526-968X(200002)26:2<149::AID-GENE16>3.0.CO;2-V

Ravikumar, B., S. Imarisio, S. Sarkar, C.J. O'Kane, and D.C. Rubinsztein. 2008. Rab5 modulates aggregation and toxicity of mutant huntingtin through macroautophagy in cell and fly models of Huntington disease. *J. Cell Sci.* 121:1649–1660. doi:10.1242/jcs.025726

Sarbassov, D.D., S.M. Ali, and D.M. Sabatini. 2005. Growing roles for the mTOR pathway. *Curr. Opin. Cell Biol.* 17:596–603. doi:10.1016/j.ceb.2005.09.009

Shin, H.W., M. Hayashi, S. Christoforidis, S. Lacas-Gervais, S. Hoepfner, M.R. Wenk, J. Modregger, S. Uttenweiler-Joseph, M. Wilm, A. Nystuen, et al. 2005. An enzymatic cascade of Rab5 effectors regulates phosphoinositide turnover in the endocytic pathway. *J. Cell Biol.* 170:607–618. doi:10.1083/jcb.200505128

Simonsen, A., and S.A. Tooze. 2009. Coordination of membrane events during autophagy by multiple class III PI3-kinase complexes. *J. Cell Biol.* 186:773–782. doi:10.1083/jcb.200907014

Sun, Q., W. Fan, K. Chen, X. Ding, S. Chen, and Q. Zhong. 2008. Identification of Barkor as a mammalian autophagy-specific factor for Beclin 1 and class III phosphatidylinositol 3-kinase. *Proc. Natl. Acad. Sci. USA.* 105:19211–19216. doi:10.1073/pnas.0810452105

Ullman, E., Y. Fan, M. Stawowczyk, H.M. Chen, Z. Yue, and W.X. Zong. 2008. Autophagy promotes necrosis in apoptosis-deficient cells in response to ER stress. *Cell Death Differ.* 15:422–425. doi:10.1038/sj.cdd.4402234

Vanhaesebroeck, B., S.J. Leevers, K. Ahmadi, J. Timms, R. Katso, P.C. Driscoll, R. Woscholski, P.J. Parker, and M.D. Waterfield. 2001. Synthesis and function of 3-phosphorylated inositol lipids. *Annu. Rev. Biochem.* 70:535–602. doi:10.1146/annurev.biochem.70.1.535

Yan, Y., R.J. Flinn, H.Y. Wu, R.S. Schnur, and J.M. Backer. 2009. hVps15, but not Ca2+/CaM, is required for the activity and regulation of hVps34 in mammalian cells. *Biochem. J.* 417:747–755. doi:10.1042/BJ20081865

Zhao, J.J., H.L. Cheng, S.D. Jia, L. Wang, O.V. Gjoerup, A. Mikami, and T.M. Roberts. 2006. The p110alpha isoform of PI3K is essential for proper growth factor signaling and oncogenic transformation. *Proc. Natl. Acad. Sci. USA.* 103:16296–16300. doi:10.1073/pnas.0607899103

Zhong, Y., Q.J. Wang, X.T. Li, Y. Yan, J.M. Backer, B.T. Chait, N. Heintz, and Z.Y. Yue. 2009. Distinct regulation of autophagic activity by Atg14L and Rubicon associated with Beclin 1-phosphatidylinositol-3-kinase complex. *Nat. Cell Biol.* 11:468–476. doi:10.1038/ncb1854

Zhou, X., L. Wang, H. Hasegawa, P. Amin, B.X. Han, S. Kaneko, Y. He, and F. Wang. 2010. Deletion of PIK3C3/Vps34 in sensory neurons causes rapid neurodegeneration by disrupting the endosomal but not the autophagic pathway. *Proc. Natl. Acad. Sci. USA.* 107:9424–9429. doi:10.1073/pnas.0914725107

Zhu, H., P. Tannous, J.L. Johnstone, Y. Kong, J.M. Shelton, J.A. Richardson, V. Le, B. Levine, B.A. Rothermel, and J.A. Hill. 2007. Cardiac autophagy is a maladaptive response to hemodynamic stress. *J. Clin. Invest.* 117:1782–1793. doi:10.1172/JCI27523